Acta Pharmaceutica Sinica B 2026;16(7):4459−4477

Chinese Pharmaceutical Association
Institute of Materia Medica, Chinese Academy of Medical Sciences

Acta Pharmaceutica Sinica B

www.elsevier.com/locate/apsb
www.sciencedirect.com

ORIGINAL ARTICLE

Scaffold hopping yields novel furo[3,2-*d*] pyrimidine NNRTIs with optimized antiviral potency, enhanced selectivity, and reduced hERG liability

Yin-Xiang Zhang[a], Christophe Pannecouque[e], Erik De Clercq[e], Enzo Tramontano[f], Angela Corona[f], Laura Dettori[f], Phuong-Thao Tran[g], Xu-Dong Li[d], Shuo Su[c], Shuai Wang[a,b,*], Fen-Er Chen[a,*]

[a]*Department of Chemistry, Engineering Center of Catalysis and Synthesis for Chiral Molecules, Shanghai Engineering Research Center of Industrial Asymmetric Catalysis of Chiral Drugs, State Key Laboratory of Green Chemical Synthesis and Conversion, Fudan University, Shanghai 200433, China*
[b]*State Key Laboratory of Natural and Biomimetic Drugs, Peking University, Beijing 100191, China*
[c]*Shanghai Institute of Infectious Disease and Biosecurity, School of Public Health, Fudan University, Shanghai 200433, China*
[d]*School of Data Science, Shanghai, Fudan University, Shanghai 200433, China*
[e]*Rega Institute for Medical Research, KU Leuven, Leuven B-3000, Belgium*
[f]*Department of Life and Environmetal Sciences, University of Cagliari, Monserrato I-09042, Italy*
[g]*Department of Pharmaceutical Chemistry, Hanoi University of Pharmacy, Hoan Kiem, Hanoi 10000, Viet Nam*

Received 10 September 2025; received in revised form 10 October 2025; accepted 4 November 2025

KEY WORDS

HIV-1;
Reverse transcriptase (RT);
Non-nucleoside RT inhibitors (NNRTIs);
Diarylpyrimidine

Abstract Considering the exceptional anti-HIV-1 potency of rilpivirine (RPV) against diverse mutant strains and its remarkable human ether-a-go-go related gene (hERG) potassium channel inhibition (IC_{50} = 0.50 μmol/L) as well as low selectivity (SI = 3989), a series of novel furo-[3,2-*d*]pyrimidine derivatives were rationally designed through a scaffold hopping strategy. Encouragingly, compound **10** revealed a striking reduction in hERG channel inhibition (IC_{50} > 30 μmol/L) and significant increase in selectivity (SI = 161580). Notably, **10** exhibited excellent antiviral activity against various HIV-1 strains (EC_{50} = 1.9−46.3 nmol/L). In particular, **10** displayed prominent inhibitory potency against

*Corresponding authors.
E-mail addresses: shuaiwang@fudan.edu.cn (Shuai Wang), rfchen@fudan.edu.cn (Fen-Er Chen).

Peer review under the responsibility of Chinese Pharmaceutical Association and Institute of Materia Medica, Chinese Academy of Medical Sciences.

https://doi.org/10.1016/j.apsb.2026.01.010

(DAPY);
Human ether-a-go-go related gene (hERG)

Y188L (EC_{50} = 15.5 nmol/L) and F227L + V106A strain (EC_{50} = 8.7 nmol/L), which was superior to those of RPV ($EC_{50\ (Y188L)}$ = 79.4 nmol/L, $EC_{50\ (F227L\ +\ V106A)}$ = 81.6 nmol/L). Besides, no apparent cytotoxicity (CC_{50} = 314.8 μmol/L) and negligible suppression of CYP isoenzymes were detected. Overall, these findings illustrated that **10** was a potentially promising NNRTI for HIV-1 therapy.

1. Introduction

Human immunodeficiency virus type 1 (HIV-1) reverse transcriptase (RT) is an attractive target, responsible for transferring viral single-stranded RNA (+ssRNA) to double-stranded DNA (dsDNA) during the HIV-1 replication cycles[1,2]. RT inhibitors are typically categorized into nucleoside RT inhibitors (NRTIs) and non-nucleoside RT inhibitors (NNRTIs)[3]. Upon non-competitive binding of NNRTIs to an allosteric pocket known as the NNRTI binding pocket (NNIBP), located approximately 10 Å from the polymerase active site where NRTIs interact, substantial constraints on the shape and conformational changes of the catalytic domain are induced resulting in final disruption of polymerase function of RT[4-6]. Compared to the first-generation NNRTIs, etravirine (**1**, ETR) and rilpivirine (**2**, RPV) as the second-generation NNRTIs have greatly improved genetic barrier towards viral resistant strains, especially for the most prevalent single mutants (K103N and Y181C) and two frequently double-mutants (RES056 and F227L + V106A), due to their "U-shaped" or "horseshoe" conformation better suited to adapt to the flexibility and plasticity of the NNIBP (Fig. 1)[7,8].

Nevertheless, diarylpyrimidine (DAPY) derivatives ETR and RPV displayed potent antiviral activity against various HIV-1 strains, their high cytotoxicity (ETR: CC_{50} > 4.6 μmol/L, RPV: CC_{50} = 4.0 μmol/L) and low selectivity (ETR: SI > 1463, RPV: SI = 3989) remained an issue[9]. In addition, serious adverse effects including hepatotoxicity and hypersensitivity reactions were frequently reported in patients receiving ETR and RPV-containing therapy[10,11]. Furthermore, RPV is highly sensitive to CYP2C9 and CYP2C19 and shows low micromolar inhibition toward CYP1A2, CYP2D6, and CYP3A4, potentially contributing to significant drug−drug interactions (DDIs) when co administrated with other drugs[12]. Moreover, in Phase IIb trials of RPV (NCT00110305), a dose-dependent prolongation of the QT intervals was observed in HIV-1-negative subjects receiving 75 and 300 mg doses, suffering from blockade of hERG potassium channel by RPV with IC_{50} values of 0.50 μmol/L[13,14]. Consequently, the risk of life-threatening arrhythmia torsades de pointes (TdP), associated with drug-induced QT interval prolongation, had narrowed the therapeutic window of RPV and limited its first-line treatment for patients with higher viral load[15].

In this work, firstly replacing the cyanovinyl group, a "Michael acceptor" of RPV with an extended biphenyl mimic, a series of novel furo[3,2-*d*]pyrimidine derivatives featuring privileged scaffold were rationally designed aiming to maintain innate flexibility of DAPY derivatives and meanwhile disrupt the planar conformation *via* scaffold hopping strategy (Fig. 2)[9,16-19]. The predicted binding mode of **7a** and HIV-1 RT indicated the two protein/solvent interfaces (the entrance channel occupied by furan ring, the tolerant region I capable of favorably accommodating various solubilizing groups). It was interesting to find out that **7a** and RPV perfectly overlapped with similar vectors. On the other hand, considering that the basic aliphatic amine of flexible piperidine ring was reported to be consequential hERG pharmacophore[20], as well as a metabolically sensitive site of the methylene linker, on the second optimization the privileged *p*-cyanoaniline group of RPV was used as scaffold again. "Fluorine- and nitrogen-walk approaches" were applied on this scaffold, theoretically attenuating the pKa value of the NH-linker on the right wing and simultaneously improving selectivity against hERG[21-23]. Moreover, these modifications may also in favor of drug-like properties of compounds.

2. Results and discussion

2.1. Chemistry

The synthetic route of the target compounds was outlined in Scheme 1. 2,4-Dichlorofuro[3,2-*d*]pyrimidine **3** could be commercially purchased or prepared according to procedures of the

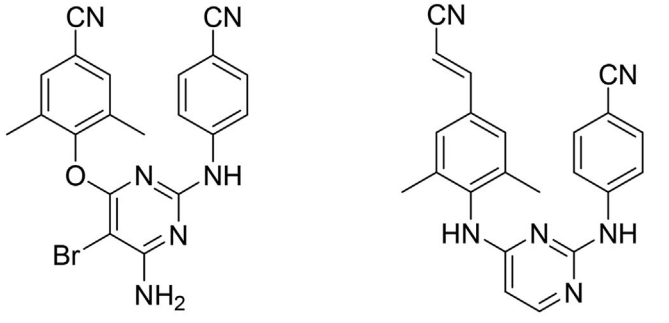

Etravirine (**1**, ETR) Rilpvirine (**2**, RPV)

Figure 1 Chemical structures of the ETR and RPV approved by the US FDA.

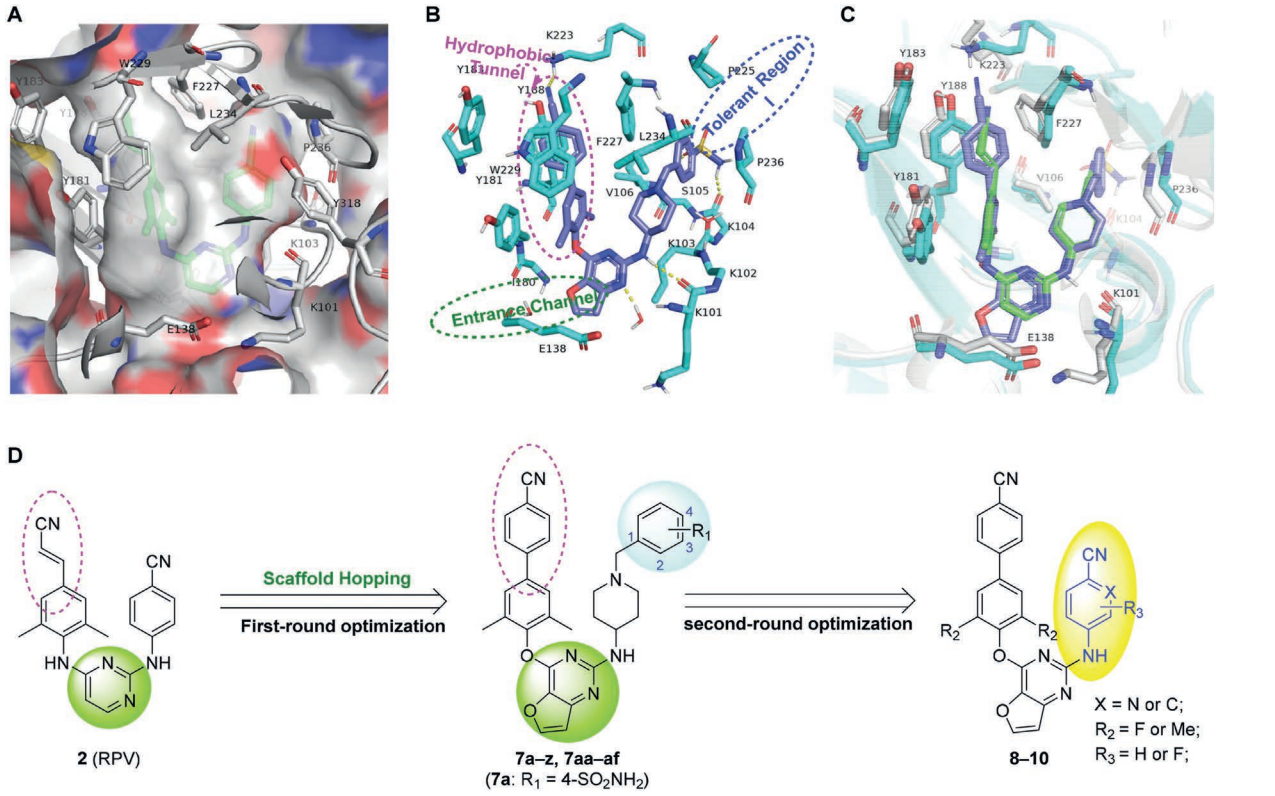

Figure 2 (A) The cocrystal complex between RPV and wild-typed (WT) HIV-1 RT (PDB ID: 2ZD1); (B) The predicted binding pattern of **7a** with WT HIV-1 RT (PDB ID: 6C0N); (C) Superposition of RPV (in green) and **7a** (in purple) coincidently overlapped highly; (D) Scaffold hopping yields novel furo[3,2-*d*]pyrimidine NNRTIs.

reference[24-26]. Starting material **3** reacted with the prepared biphenol in DMF with K_2CO_3 as a base to afford **4** in excellent yield. Treament of **4** in excess *N*-Boc-4-aminopiperidine and then heated to 120 °C with no solvents to furnish **5**. Then **5** was subjected to trifluoroactic acid (TFA) in dichloromethane to obtain common intermediate **6**, followed by diverse substituted benzyl bromide or chloride to afford the target compounds **7a**−**z** and **7aa**−**af**. On the other hand, Buchwald coupling step efficiently produced the target compounds **8**−**10** on the intermediate **4** or its analog[27,28].

2.2. *In vitro HIV-1 inhibition activity and cytotoxicity*

Initially, the antiviral activities of 35 compounds against the WT HIV-1 strain (IIIB) and the double mutant strain K103N + Y181C (RES056) in infected MT-4 cell cultures were assessed employing the MTT assay[29]. Subsequently, promising derivatives were further selected to evaluate their efficacy against five single mutant strains (L100I, K103N, Y181C, Y188L, E138K) and the double-mutant strain (F227L + V106A). Nevirapine (NVP), efavirenz (EFV), ETR and RPV were selected as reference drugs. Their biological outcomes were determined by the EC_{50} (anti-HIV-1 activity), CC_{50} (cytotoxicity) and SI (selectivity index, the ratio of CC_{50}/EC_{50}) values.

As shown in Table 1, the terminal sulfonamide was replaced by a variety of hydrophilic and hydrophobic groups, simultaneously hydrogen-bond donors or acceptors in most cases. The preliminary structure and activity relationship (SAR) was relatively clear as follows. The novel derivatives (**7a**−**m**, **7aa**−**af**) displayed moderate to potent antiviral activities towards WT HIV-1 strain (EC_{50} = 6.1−385.8 nmol/L). Concretely, sulfonamide **7a** showed potent antiviral activity ($EC_{50\ (WT)}$ = 6.3 nmol/L, $EC_{50\ (RES056)}$ = 196.9 nmol/L) and high cytotoxicity (CC_{50} = 1.0 μmol/L). Inspired by a "magic methyl effect", the methylation derivative **7b** exhibited a 3-fold reduction in potency than **7a** and its methyl sulfone analog **7c** retained its activity (EC_{50} = 7.8 nmol/L), both of which dramatically lost their efficacy against RES056 mutant strain. In contrast, amide **7d** and methyl amide **7e** showed comparable activity against WT strain (EC_{50} = 6.1 or 7.5 nmol/L) and only a modest reduction in potency against RES056 strain, so did hydroxylmethyl analog **7f**. Meanwhile, when the substitutes were ketone, ester, nitro, trifluoromethyl, halogen atoms like bromine or chlorine, or methyl (**7g**−**m**), the potency of these compounds decrease by 5.9- to 56-fold reduction compared to **7a**, and loss of antiviral activity against RES056 strain. Furthermore, the substitute position on the benzene group played a critical role in their potency, namely 4′-postion >2′-position >3′-position. The 4-CN substitute **7aa** (EC_{50} = 34.4 nmol/L) exhibited 1.3-fold stronger inhibitory effect than 2-CN substitute **7ac**, remarkably 11.2-fold more potent than 3-CN substitute **7 ab**. A similar trend was observed in the pyridine ring in place of benzene ring (**7ad**, **7ae**, **7af**). More notably, **7ad** displayed superior potency both against the WT and RES056 strain than **7aa**. The observed differences in potency may be attributed to the fact that the pyridine ring was situated in closer proximity to the protein-binding region, whereas the 4-CN moiety extended toward a more solvent-exposed region, thereby reducing the binding contribution of **7aa**. The SAR analysis indicated that

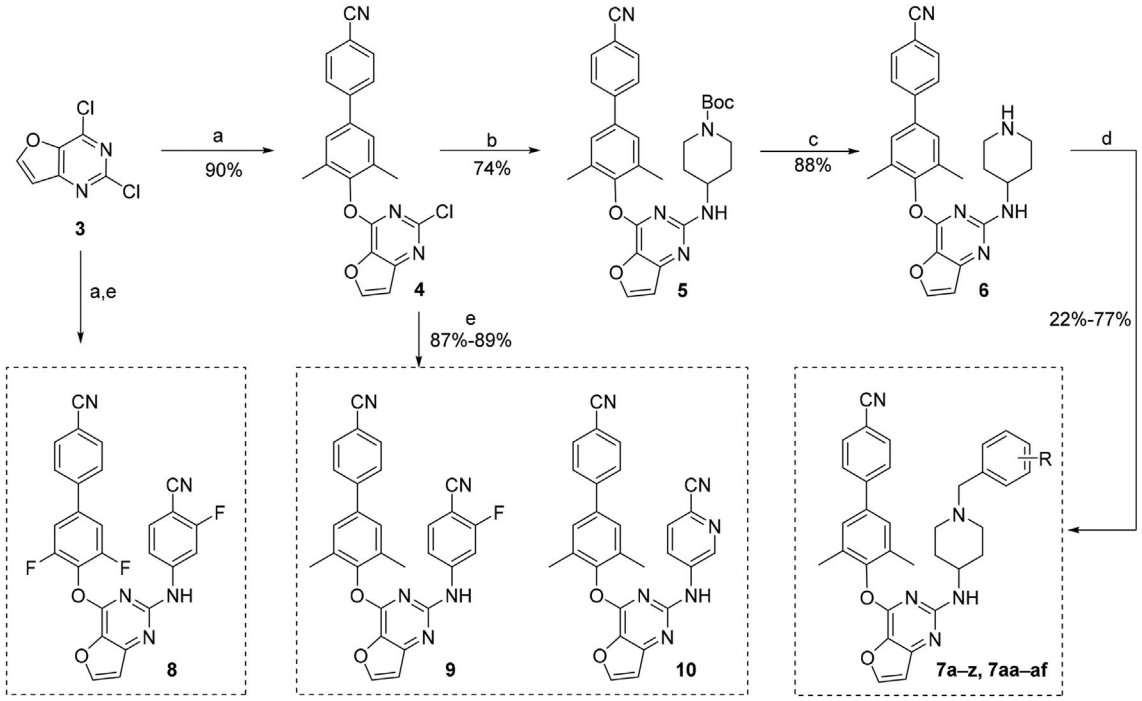

Scheme 1 Synthesis of target compounds. Reagents and conditions: (a) substituted phenols, DMF, K_2CO_3, rt, 2 h; (b) *N*-Boc-4-aminopiperidine, neat, 120 °C, 10 h; (c) TFA, DCM, rt, 4 h; (d) substituted benzyl bromide or chlorine, DMF, K_2CO_3, rt, 4−12 h. (e) $Pd_2(dba)_3$, BINAP, dioxane, Cs_2CO_3, N_2, 100 °C, 12 h.

hydrophilic substituents were generally more favorable than lipophilic ones. Among the evaluated compounds, **7a**, **7d,** and **7e** were considered to exhibit acceptable inhibitory activity against the RES056 strain.

Next, 13 newly analogues (**7n**−**z**) varied in space, size and electronic nature were designed and evaluated to explore the effect of extending hydrophilic groups protruded into the solvent-exposed regions. As depicted in Table 2, displacement of amine of **7d** with a morpholine ring afforded **7n**, which showed a moderate decline in antiviral efficacy both against WT HIV-1 and RES056 strain. Thiomorpholine ring (**7o**), pyrrole ring (**7p**) and 2-thiophenemethyl moiety (**7q**) replacement further reduced their potency, which might be attributed to their increased lipophilicity, though anticipated partial protonation under physiological conditions to enhance solubility and absorption. Amide **7r** featuring a terminal hydroxyl-piperidine ring was in line with the expectation that exhibited an elevated inhibition both towards WT (EC_{50} = 7.6 nmol/L) and RES056 (EC_{50} = 391.0 nmol/L). **7s** had a $EC_{50\ (WT)}$ of 13.2 nmol/L. Sulfuryl analogs as a bioisosteric replacement of carbonyl amide were also explored. **7t** showed a slight increase in potency against WT and a 5-fold reduction against RES056 than analog **7p**. Concomitant decline in efficacy against WT and RES056 was observed in **7u**. Taking into account less steric hindrance, different lengths of linear hydrophilic substitutes were evaluated. It was noteworthy that **7v**−**7z** displayed robust inhibitory activity ($EC_{50\ (WT)}$ = 4.8−18.7 nmol/L). Endowed with a methoxy-ethyl-amide appendage, **7w** restored its activity ($EC_{50\ (WT)}$ = 8.6 nmol/L, $EC_{50\ (RES056)}$ = 149.9 nmol/L), surpassing NVP ($EC_{50\ (RES056)}$ > 15.0 μmol/L) and EFV ($EC_{50\ (RES056)}$ = 394.6 nmol/L), however inferior to ETR ($EC_{50\ (RES056)}$ = 59.1 nmol/L) and RPV ($EC_{50\ (RES056)}$ = 10.7 nmol/L). Liner sulfuryl amide analogs **7y** and **7z** were also in accordance with this tendency, though did not improve their potency against RES056. Nevertheless, all evaluated derivatives displayed low CC_{50} values, indicating their high cytotoxicity. Additionally, these observations concluded that hydrophilic groups extending to the solvent-exposed regions were beneficial to their anti-HIV-1 activities (WT and RES056) than lipophilic groups. Not surprisingly liner hydrophilic substituents were preferable over groups with bulky steric hindrance.

On the second modification, replacement of amine-piperidine ring on the right wing with modified *p*-cyanoaniline fragment of RPV afforded **8**−**10**. compound **8** harboring difluorobiphenyl motif presented potent activity against WT HIV-1 and a high safety profile as expected. However, it was largely inactive against the RES056 strain hinting the importance of the dihedral angels. To our delight, compounds **9** and **10**, with decoration of a fluorine or a nitrogen atom on the scaffold, not only displayed the robust antiviral activities (**9**: $EC_{50\ (WT)}$ = 4.5 nmol/L, $EC_{50\ (RES056)}$ = 24.3 nmol/L; **10**: $EC_{50\ (WT)}$ = 1.9 nmol/L, $EC_{50\ (RES056)}$ = 46.3 nmol/L), being comparable to ETR ($EC_{50\ (WT)}$ = 3.1 nmol/L, $EC_{50\ (RES056)}$ = 59.1 nmol/L) and RPV ($EC_{50\ (WT)}$ = 1.0 nmol/L, $EC_{50\ (RES056)}$ = 10.7 nmol/L), but also demonstrated low cytotoxicity and high selectivity index (**9**: CC_{50} = 275.4 μmol/L, SI = 60,898 and **10**: CC_{50} = 314.8 μmol/L, SI = 161,580). These finding aligned with structure-based drug design principles and have guided the rational development of promising compounds as potential NNRTIs.

2.3. Inhibitory activities of representative compounds against HIV-1 mutant strains

Based on the preeminent inhibitory potency against WT and RES056 strains, those promising compounds were selected to further evaluate their ability to inhibit a range of NNRTI-resistant mutations, including single mutants L100I, K103N, Y181C, Y188L, E138K and double mutant F227L + V106A. As shown in Table 3, these

Table 1 Activity and cytotoxicity of **7a**−**m**, **7aa**−**af** in MT-4 cells.

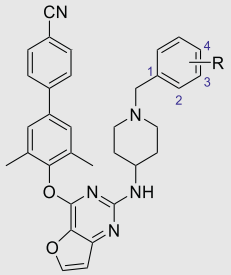

Compd.	R	EC_{50} (nmol/L)[a]		CC_{50} (μmol/L)[b]	SI (III_B)[c]
		IIIB	RES056		
7a	4-SO_2NH_2	6.3 ± 2.0	196.9 ± 8.3	1.0 ± 0.5	160
7b	4-SO_2NHCH_3	18.3 ± 13.0	>208.7	1.3 ± 0.4	73
7c	4-SO_2CH_3	7.8 ± 3.7	>625.7	0.6 ± 0.6	80
7d	4-$CONH_2$	6.1 ± 2.7	622.0 ± 468.8	3.4 ± 0.5	556
7e	4-$CONHCH_3$	7.5 ± 1.5	247.9 ± 93.5	3.4 ± 0.5	446
7f	4-CH_2OH	9.0 ± 4.4	>125.0	1.7 ± 0.2	190
7g	4-$COCH_3$	37.2 ± 23.4	>3865.7	3.9 ± 2.3	104
7h	4-COOMe	285.9 ± 149.4	33,538.7 ± 3452.0	60.7 ± 19.8	212
7i	4-NO_2	112.1 ± 132.8	>2662.5	2.7 ± 2.6	24
7j	4-CF_3	331.4 ± 317.2	>4250.0	4.2 ± 3.4	13
7k	4-Br	351.2 ± 218.1	>15,090.0	15.1 ± 10.9	43
7l	4-Cl	318.0 ± 184.2	>15,130.0	15.1 ± 9.2	48
7m	4-CH_3	309.0 ± 345.3	>36,780	>36.78	>119
7aa	4-CN	34.4 ± 7.1	>1057.0	1.1 ± 0.6	31
7 ab	3-CN	385.8 ± 436.2	>5899.9	5.9 ± 0.7	15
7ac	2-CN	45.8 ± 9.5	8493.1 ± 598.9	21.1 ± 18.6	461
7ad	4′-Py	11.1 ± 5.5	697.7 ± 513.6	3.1 ± 2.6	284
7ae	3′-Py	20.8 ± 16.1	6662.9 ± 844.6	8.2 ± 3.7	393
7af	2′-Py	34.5 ± 13.8	8531.2 ± 1009.1	11.0 ± 2.5	320
NVP		186.7 ± 68.8	>15,000	>15.0	>81
EFA		4.1 ± 1.0	394.6 ± 17.0	>6.3	>1538
ETR		3.1 ± 0.8	59.1 ± 47.0	>4.6	>1463
RPV		1.0 ± 0.3	10.7 ± 8.0	4.0	3989

[a]EC_{50}: The effective concentration required to protect MT-4 cells against HIV-induced cytopathogenicity by 50%.
[b]CC_{50}: The cytotoxic concentration of the compound that reduced the normal uninfected MT-4 cell viability by 50%.
[c]SI: selectivity index, the ratio CC_{50}/EC_{50} (WT).

compounds collectively maintained significant broad-spectrum activity at low nanomolar levels against various mutant strains. As for L100I strain, **10** provided the greatest efficacy (EC_{50} = 8.1 nmol/L), which was 49-fold more potent than EFV (EC_{50} = 393.6 nmol/L) and comparable to ETR (EC_{50} = 8.0 nmol/L). Taking into account K103N strain, the most prevalent single mutant, it was noticeable that all tested compounds displayed exceptional potency (EC_{50} = 4.1−8.5 nmol/L), substantially outperforming NVP (EC_{50} = 6464.7 nmol/L), EFV (EC_{50} = 76.9 nmol/L) and comparable to ETR (EC_{50} = 3.1 nmol/L) and RPV (EC_{50} = 1.31 nmol/L). With regard to Y181C and Y188L strains that involved in significant aryl−aryl stacking contacts with small molecules, tested compounds were still endowed with prominent activity with ($EC_{50\,(Y181C)}$ = 11.5−39 nmol/L, $EC_{50\,(Y188L)}$ = 15.3−98 nmol/L). In the case of E138K strain greatly emerging from the failure of RPV-containing regimens, the most potent inhibitor **10** (EC_{50} = 6.6 nmol/L) demonstrated marginally superior inhibitory potency to ETR (EC_{50} = 12.5 nmol/L). Considering that the F227L + V106A mutant confers significantly reduced susceptibility to NVP and EFV, **10** exhibited notable inhibitory activity (EC_{50} = 8.7 nmol/L), which was 31.7-fold more potent than EFV (EC_{50} = 276.0 nmol/L) and 9.4-fold than RPV (EC_{50} = 81.6 nmol/L). To our delight, the RF values of these compounds were also encouraging. For example, their RF values for K103N was ranging from 0.9 to 2.2, indicating these novel compounds are more resilient to the K103N mutant. Especially for Y181C and F227L + V106A mutants, **10** displayed exceedingly improved anti-resistance profile (RF = 8.2 and 4.6, respectively) over RPV (RF = 79.4 or 81.6, respectively). Taken together, these results confirmed the privileged scaffold of dimethylbiphenyl fragment and modified *p*-cyanopyridylaniline moiety in balancing potency and cytotoxicity, indicating **10** as the most potential compound.

Table 2 Activity and cytotoxicity of **7n**−**z** and **8**−**10** in MT-4 cells.

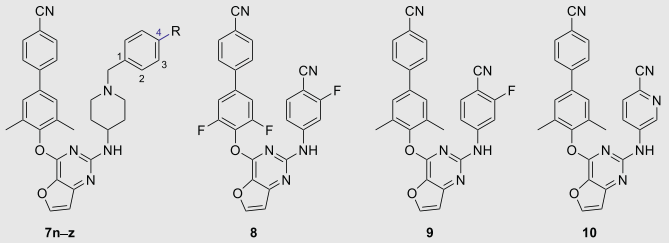

Compd.	R	EC_{50} (nmol/L)[a]		CC_{50} (μmol/L)[b]	SI (III_B)[c]
		IIIB	RES056		
7n	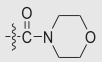	13.1 ± 6.8	>1166.8	1.2 ± 0.4	89
7o	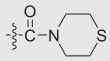	24.1 ± 13.5	1197.7 ± 8.7	1.8 ± 0.2	73
7p		35.9 ± 28.7	1448.2 ± 318.5	9.7 ± 5.7	270
7q	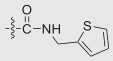	38.5 ± 17.7	795.4 ± 80.0	3.6 ± 0.9	94
7r	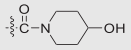	7.6 ± 6.1	391.0 ± 122.2	3.4 ± 0.5	450
7s	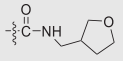	13.2 ± 13.1	>228.3	1.1 ± 0.4	82
7t		27.1 ± 9.9	7775.5 ± 186.5	3.3 ± 3	123
7u	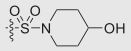	22.3 ± 4.6	1065.8 ± 85.7	0.5 ± 0.5	21
7v	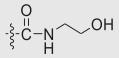	7.5 ± 4.5	187.3 ± 29.8	5.7 ± 1.9	763
7w	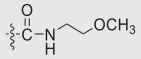	8.6 ± 1.2	149.9 ± 21.6	2.2 ± 0.3	260
7x	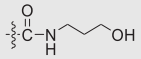	4.8 ± 1.8	373.2 ± 90.1	2.3 ± 0.5	487
7y	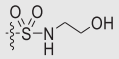	18.7 ± 8.9	>398.3	0.4 ± 0.4	22
7z	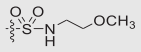	14.7 ± 7.4	>944.8	0.5 ± 0.5	34
8		12.0 ± 2.2	5978.4 ± 0	492.1 ± 63.1	40,836
9		4.5 ± 4	24.3 ± 1.6	275.4 ± 36.4	60,898
10		1.9 ± 0.1	46.3 ± 30.4	314.8 ± 28.0	161,580
NVP		186.7 ± 68.8	>15,000	>15.0	>81
EFA		4.1 ± 1.0	394.6 ± 17.0	>6.3	>1538
ETR		3.1 ± 0.8	59.1 ± 47.0	>4.6	>1463
RPV		1.0 ± 0.3	10.7 ± 8.0	4.0	3989

[a]EC_{50}: The effective concentration required to protect MT-4 cells against HIV-induced cytopathogenicity by 50%.
[b]CC_{50}: The cytotoxic concentration of the compound that reduced the normal uninfected MT-4 cell viability by 50%.
[c]SI: selectivity index, the ratio CC_{50}/EC_{50} (WT).

2.4. In vitro inhibitory activity against WT HIV-1 RT

The inhibitory efficacy of all compounds **7a**−**7z**, **7aa**−**af** and **8**−**10** was also investigated utilizing NVP, EFV, ETR and RPV as benchmarks. As summarized in Table 4, all compounds demonstrated moderate inhibitory potency against WT HIV-1 RT (IC_{50} = 0.050−0.810 μmol/L), being superior to NVP (IC_{50} = 1.090 μmol/L). Collectively, these compounds were considered to be identified as NNRTIs by binding to HIV-1 reverse transcriptase. It was palpable that the most derivatives behaved higher cellular inhibition activity than those in enzyme assays. The existed discrepancies may be attributed to template-specific

Table 3 Antiviral activity of selected compounds against HIV-1 mutant strains.

Compd.	EC_{50} (nmol/L)[a] (resistance fold)[b]					
	L100I	K103N	Y181C	Y188L	E138K	F227L + V106A
7a	22.1 ± 6.3 (3.5)	5.8 ± 1.1 (0.9)	26.3 ± 6.4 (4.2)	43.0 ± 13.7 (6.8)	28.2 ± 3.6 (4.5)	35.5 ± 10.6 (5.6)
7d	49.0 ± 11.8 (8.0)	8.5 ± 2.4 (1.4)	38.6 ± 3.8 (6.3)	58.6 ± 16.8 (9.6)	39.9 ± 14.4 (6.5)	90.5 ± 18.0 (14.8)
7e	40.5 ± 4.3 (5.4)	8.3 ± 1.6 (1.1)	34.1 ± 3.0 (4.5)	45.2 ± 15.6 (6)	31.3 ± 8.9 (4.2)	51.2 ± 12.3 (6.8)
7r	16.0 ± 2.1 (2.1)	6.3 ± 1.9 (0.8)	27.1 ± 11.8 (3.6)	98.0 ± 41.2 (12.9)	19.5 ± 3.0 (2.6)	42.8 ± 11.1 (5.6)
7v	41.7 ± 10.8 (5.6)	8.4 ± 1.5 (1.1)	39.0 ± 5.3 (5.2)	47.6 ± 15.8 (6.3)	42.6 ± 11.1 (5.7)	56.9 ± 15.1 (7.6)
7w	25.5 ± 7.2 (3.0)	7.6 ± 1.4 (0.9)	22.0 ± 4.2 (2.6)	43.6 ± 5.9 (5.1)	23.5 ± 6.0 (2.7)	39.3 ± 17.2 (4.6)
7x	53.1 ± 30.5 (11.1)	5.4 ± 1.7 (1.1)	19.1 ± 3.1 (4.0)	81.0 ± 33.7 (16.9)	22.2 ± 7.1 (4.6)	198.1 ± 160.5 (41.3)
9	10.1 ± 5.2 (2.2)	6.6 ± 7.2 (1.5)	13.3 ± 3.2 (3.0)	19.3 ± 7.0 (4.3)	14.2 ± 5.3 (3.2)	14.8 ± 13.6 (3.3)
10	8.1 ± 1.3 (4.3)	4.1 ± 2.3 (2.2)	14.4 ± 11.1 (7.6)	15.5 ± 3.6 (8.2)	6.6 ± 1.7 (3.5)	8.7 ± 1.4 (4.6)
NVP	2000.2 ± 1385.3 (10.7)	6464.7 ± 2995.6 (34.6)	7147.6 ± 1325.0 (38.3)	>15,000 (>80.3)	153.3 ± 55.3 (0.8)	>15,000 (>80.3)
EFA	393.6 ± 17.0 (96.0)	76.9 ± 20.0 (18.8)	8.2 ± 3.3 (2.0)	277.8 ± 51.0 (67.8)	7.8 ± 2.5 (1.9)	276.0 ± 270.0 (67.3)
ETR	8.0 ± 6.0 (2.6)	3.1 ± 1.1 (1.0)	15.8 ± 5.2 (5.1)	23.9 ± 7.1 (7.7)	12.5 ± 8.9 (4)	8.7 ± 3.0 (2.8)
RPV	1.5 ± 0.0 (1.5)	1.3 ± 0.4 (1.3)	4.7 ± 0.5 (4.7)	79.4 ± 0.8 (79.4)	5.8 ± 0.1 (5.8)	81.6 ± 21.2 (81.6)

[a]EC_{50}: The effective concentration required to protect MT-4 cells against HIV-induced cytopathogenicity by 50%.
[b]Resistance fold: RF, ratio of EC_{50} against mutant strain/EC_{50} against WT strain.

variations in HIV-1 RT binding affinity and processivity, metabolic transformation or activation, or enhanced cellular uptake leading to increased intracellular concentrations.

2.5. Molecular docking analysis

To gain insights into variations in antiviral activity of compounds against various HIV-1 strains, the molecular docking modes of two representative compounds **7w** and **10** within the NNIBP of RT were studied. The X-ray crystal structures of HIV-1 WT RT (PDB ID: 6C0N or 2ZD1), two double-mutant strains RES056 RT (PDB ID: 6C0R) and F227L + V106A RT (PDB ID: 6DUF) were served as input structures and processed by Schrödinger Maestro 11.4. The ultimate docking results were visualized by PyMOL 1.5.

Table 4 Inhibitory activity of all compounds against WT HIV-1 RT.

Compd.	IC_{50} (μmol/L)[a]	Compd.	IC_{50} (μmol/L)[a]
7a	0.330 ± 0.060	**7af**	0.587 ± 0.199
7b	0.365 ± 0.047	**7n**	0.540 ± 0.207
7c	0.431 ± 0.042	**7o**	0.430 ± 0.017
7d	0.392 ± 0.063	**7p**	0.639 ± 0.191
7e	0.271 ± 0.057	**7q**	0.390 ± 0.031
7f	0.416 ± 0.023	**7r**	0.528 ± 0.154
7g	0.351 ± 0.043	**7s**	0.461 ± 0.014
7h	0.488 ± 0.169	**7t**	0.461 ± 0.048
7i	0.262 ± 0.016	**7u**	0.355 ± 0.033
7j	0.798 ± 0.047	**7v**	0.430 ± 0.014
7k	0.767 ± 0.087	**7w**	0.402 ± 0.026
7l	0.542 ± 0.129	**7x**	0.419 ± 0.042
7m	0.810 ± 0.118	**7y**	0.538 ± 0.024
7aa	0.270 ± 0.015	**7z**	0.461 ± 0.075
7 ab	0.243 ± 0.031	**8**	0.099 ± 0.021
7ac	0.308 ± 0.013	**9**	0.055 ± 0.012
7ad	0.348 ± 0.049	**10**	0.050 ± 0.012
7ae	0.431 ± 0.124	ETR	0.029 ± 0.005
NVP	1.090 ± 0.39	RPV	0.035 ± 0.005
EFA	0.013 ± 0		

[a]IC_{50}: half-inhibitory concentration of test compounds against WT HIV-1 RT.

As shown in Fig. 3A, Compound **7w** was favorably repositioned within NNIBP to adopt a horseshoe-like conformation closely resembling that of classical NNRTIs. Compared to RPV, **7w** was encouragingly not affected by slight change of NNIBP caused by F227L + V106A double mutation. The decreased hydrophobic interactions could be probably compensated by the newly developed water-mediated hydrogen bonds between basic amine on piperidine ring with carbonyl oxygen of P236 and amide nitrogen of K103 (Fig. 3B). However, **7w** did not retain potent efficacy against the RES056 mutant strain, primarily due to its larger alterations of NNIBP. It was noteworthy that Y183, a residue in the conserved YMDD motif at the polymerase active site underwent a significant positional shift and moved about 2.4 Å away from the initial position of Y183 in docking mode of WT RT, which meant hardly π-contact compensation resulting **7w** in a little decrease in potency (Fig. 3C).

To luminate the rationale of **10** with the exceptional inhibitory activity, the binding modes of **10** with RT were also analyzed. As shown in Fig. 4A−C, the smaller structure of **10** was inserted into the active binding pocket adapting to a classical "U" shape conformation, similar to RPV. Most importantly, two typical hydrogen bonds were persistently maintained between the N atom of pyrimidine scaffold and carbonyl NH of K101, as well as NH-linker with carbonyl oxygen atom of K101. Intriguingly, the furo[3,2-*d*]pyrimidine central ring of **10** established two salt bridges with the side chain amine of residue K101 in F227L + V106A mutant strain, which might be the reason why the activity of **10** was 5.3-fold higher than that in RES056 mutant strain. Another indispensable binding forces including hydrophobic interaction, electrostatic and van der Waals were also responsible for its high potency.

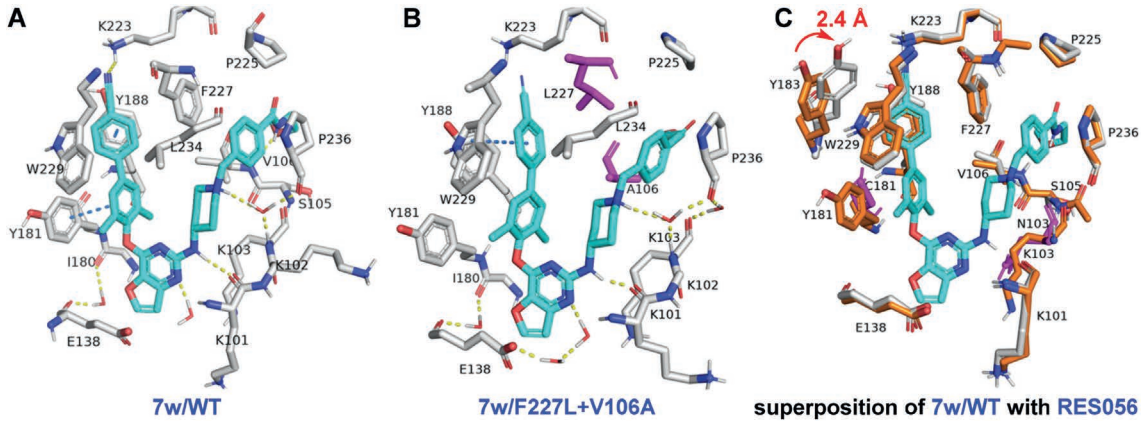

Figure 3 (A) Predicted binding pattern between **7w** (cyan) and WT HIV-1 RT (PDB ID: 6C0N); (B) F227L + V106A (PDB ID: 6DUF); (C) superposition of **7w**/WT (gray) with RES056 (orange, PDB ID: 6C0R). Mutated residues are depicted as magentas stick. Hydrogen bonds are showed as yellow dashed lines and $\pi-\pi$ stacking contacts are illustrated as marine dashed lines.

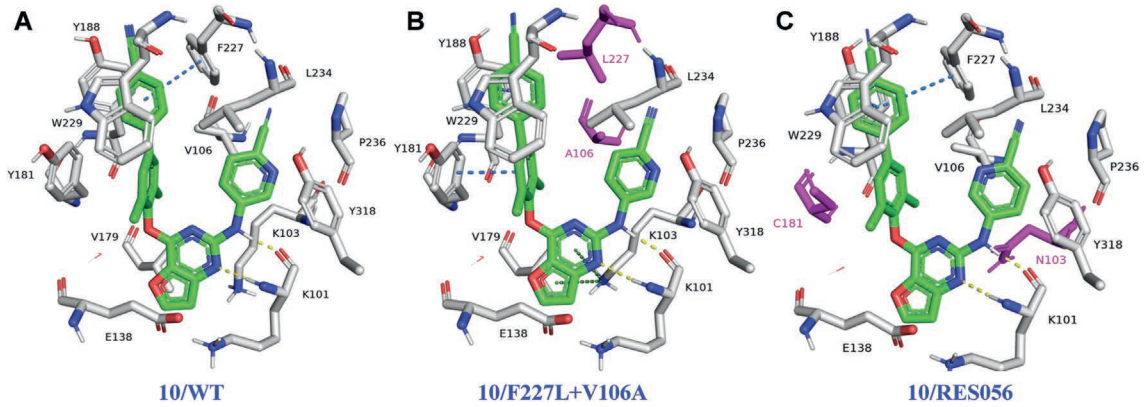

Figure 4 (A) Predicted binding pattern between **10** (green) and WT HIV-1 RT (PDB ID: 2ZD1); (B) RES056; (C) F227L + V106A; Site-directed mutations derive from WT HIV-1 RT and mutated residues are depicted as magentas stick. Hydrogen bonds are showed as yellow dashed lines, $\pi-\pi$ stacking contacts as marine dashed lines and salt bridges are illustrated as dark-green dashed lines.

2.6. *Molecular dynamic simulations*

To gain further insights into the dynamic interactions, the binding and conformational stability of compounds **7w** and **10** in WT HIV-1 RT allosteric pockets (PDB ID: 6C0N and 2ZD1, respectively) were explored through molecular dynamic (MD) simulations spanning 100 ns in Schrödinger Maestro 11.4. As depicted in Figs. 5A and 6A, the root mean square deviation (RMSD) of the protein (left *Y*-axis) indicated its structural conformation, and RMSD of the ligand (right *Y*-axis) indicated how stable the ligand was with respect to the protein and its binding pocket. Their RMSD values both remained below 3 Å, indicating the protein/ligand (RT/**7w** or RT/**10**) complex rapidly stabilized during equilibration and maintained strong bindings so that the ligand seemed impossible to diffuse away from the binding site. Fig. 5B and C and 6B, C illustrate the simulated interaction modes of the two complex in detail. Several main interactions types were observed in protein/ligand complex: hydrogen bonding, hydrophobic interaction, ionic, water bridges and halogen bonding. The value of the interaction fraction suggested the probability of the occurrence of a specific contact during the simulation time. Values exceed 1.0 was possible, as some protein residue may form multiple contacts with the ligand. Corresponding to our previous results, in RT/**7w** complex, K101 (LYS101) indicated by a deep hue of orange within the trajectory frame consistently formed the distinguished hydrogen bond with the NH linker of **7w** on the right wing and water-bridged hydrogen bond with N1 nitrogen on its furo[3,2-*d*]pyrimidine scaffold. Additionally, **7w** consistently established two water-bridged hydrogen bonds with Q222 (GLN222) and E138 (GLU138). Hydrophobic interactions between **7w** and certain backbone amino residues, namely L100 (LEU100), V106 (VAL106), V179 (VAL179), Y188 (TYR188), F227 (PHE227), W229 (TRP229), L234 (LEU234) and Y318 (TYR318) were also observed during the simulation time. In RT/**10** complex, K101 (LYS101) engaged in an important hydrogen bond with the NH linker of **10** on the right wing for approximately 100% of the simulation time, and with the N1 nitrogen on the furo[3,2-*d*]pyrimidine skeleton for almost 85% duration. Moreover, distinct water-bridged hydrogen bonds between **10** and residues like K103 (LYS103), L228 (LEU228) and P236 (PRO236) were found. Similarly, predominate $\pi-\pi$ contacts were consistently observed between Y188 (TYR188) or highly conserved W229 (TRP229) and the biphenyl fragment of **10** for nearly entire

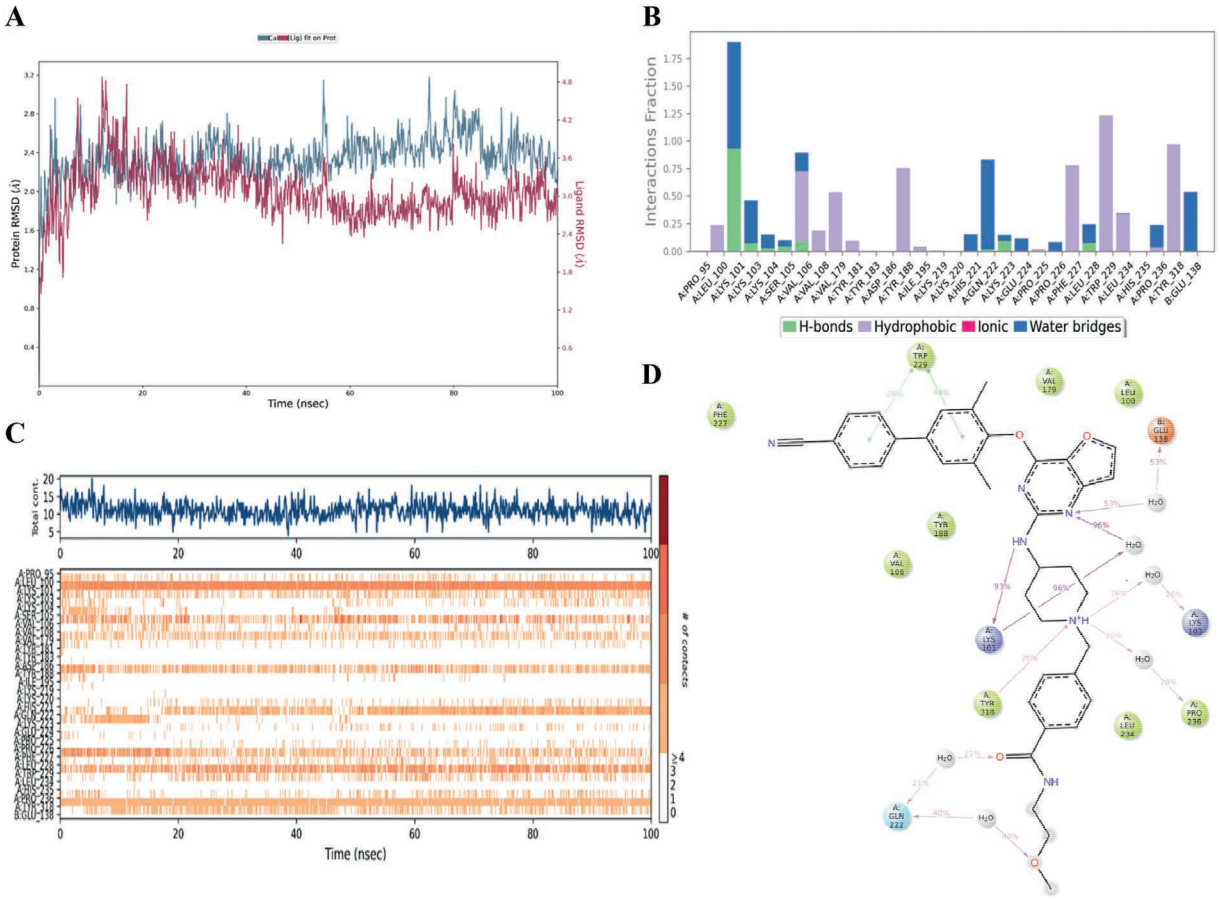

Figure 5 Molecular dynamics simulations analysis between **7w** and WT HIV-1 RT (PDB ID: 6C0N). (A) Protein−ligand RMSD indicates the stability of the model; (B−D) Monitoring of protein−ligand contacts throughout MD trajectories.

trajectory. All these interactions were deemed to stabilize the protein/ligand complex.

2.7. *Effect of **10** on hERG activity*

The drug-induced blockade of the hERG-associated potassium current is recognized as a primary cause of drug-induced arrhythmias in humans. RPV has been reported as a potent hERG potassium channel inhibitor (IC_{50} = 0.50 μmol/L). To assess the potential cardiac toxicity of **10**, we conducted the relevant assay with **10** in CHO-hEGR cells, cisapride as postivie control. As depicted in Fig. 7, compound **10** showed no significant inhibition towards hEGR (IC_{50} > 30 μmol/L), tremendously lower than that of the positive agent cisparide (IC_{50} = 0.04 μmol/L). The data provided evidence for **10** as a secure NNRTIs.

2.8. *Effect of **10** on CYP enzyme inhibitory activity*

Since ETR is an inhibitor of CYP2C9, CYP2C19 as well as an inducer of CYP3A4, and RPV acts as an inhibitor of CYP3A4, potentially contributing to significant DDIs when co-administrated with other medications. Compound **10** was assessed for its inhibitory activity on six major CYP isoenzymes depicted in Table 5. **10** displayed no detectable inhibitory potency against the tested isoforms (CYP1A2, CYP2D6, CYP3A4-M, and CYP3A4-T) as IC_{50} values consistently greater than 50 μmol/L. Meanwhile, **10** showed marginal inhibition toward CYP2C19 and CYP2C9 (IC_{50} = 36.3 and 22.7 μmol/L, respectively), which was 108- and 65.6-fold less potent than that of RPV. These findings demonstrated that 10 was less prone to induce DDIs.

2.9. *In vivo pharmacokinetics study*

The pharmacokinetic (PK) profiles of **10** in Sprague−Dawley rats were assessed after administration of a single intravenous (iv) and oral administration (*po*), respectively. The variation of plasma concentration-time of **10** was depicted in Fig. 8. At the circumstance of iv administration, the plasma concentration started to decline from the T_0 point. Whereas following oral dosing, the plasma concentration initially increased to a maximum value before gradually decrease. This pattern indicated that **10** was rapidly absorbed into the plasma and then slowly eliminated *via* metabolic processes. The detailed PK data were summarized in Table 6, after intravenous administration at 1.0 mg/kg, **10** exhibited a half-life ($t_{1/2}$) of 1.48 h and reached the maximum concentration (C_{max}) at 2215 ng/mL. Additionally, the area under the plasma concentration−time curve ($AUC_{0-\infty}$) of 922 h ng/mL and moderate clearance (CL = 1114 mL/h/kg) were detected. When **10** was administered orally at a dose of 10.0 mg/kg, $t_{1/2}$ was prolonged to 4.14 h, the C_{max} of 126 ng/mL was attained at 2.33 h

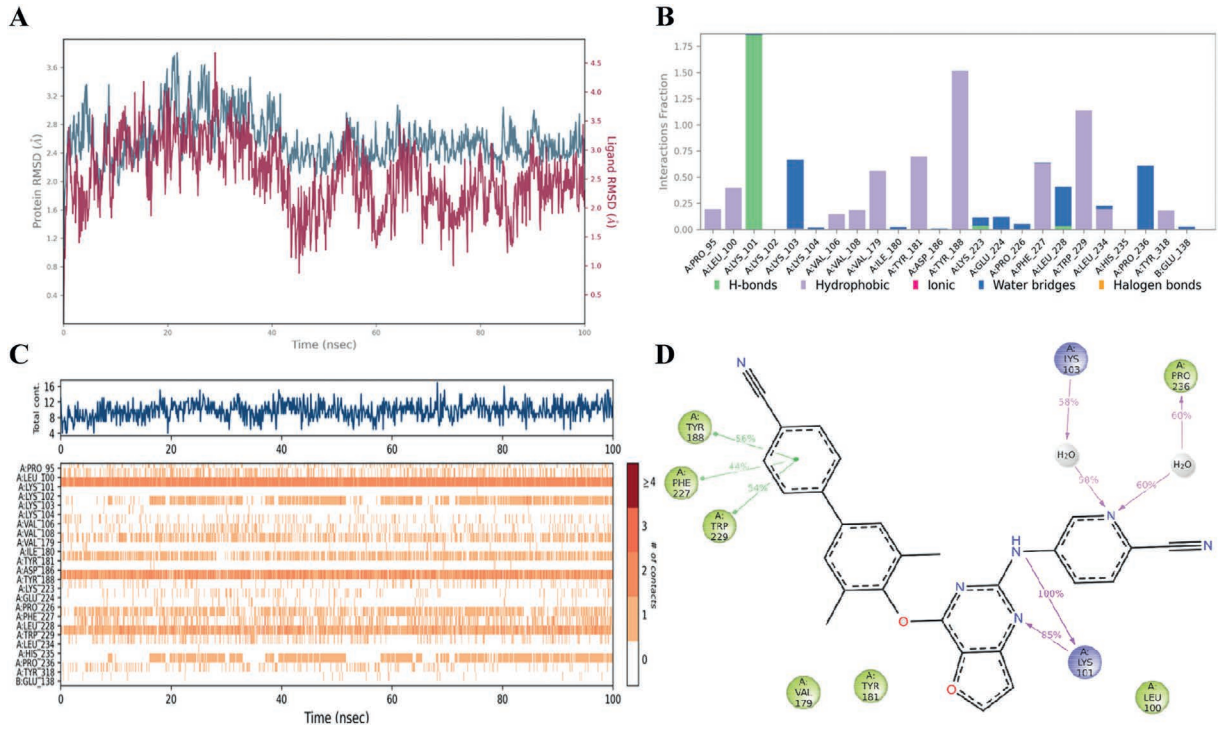

Figure 6 Molecular dynamics simulations analysis between **10** and WT HIV-1 RT (PDB ID: 2ZD1). (A) Protein−ligand RMSD indicates the stability of the model; (B−D) Monitoring of protein−ligand contacts throughout MD trajectories.

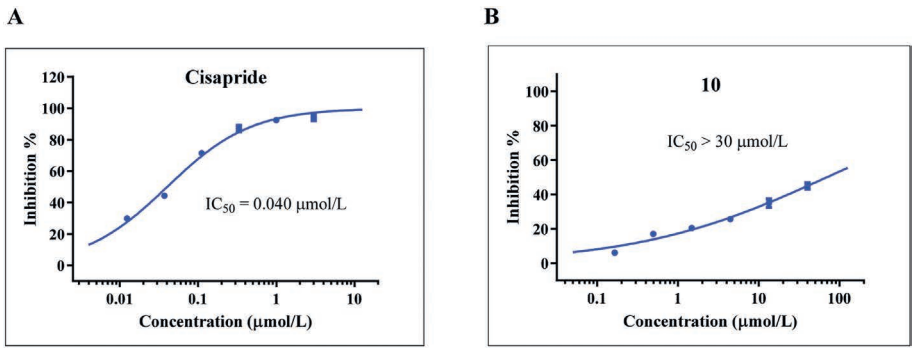

Figure 7 Effect of **10** (A) and cisapride (B) on hERG in CHO-hERG cells.

Table 5 Inhibitory activity of **10** against Six CYP isoenzymes.

Compd.	IC_{50} (μmol/L)[h]					
	CYP1A2	CYP2C19	CYP2C9	CYP2D6	CYP3A4-M	CYP3A4-T
10	>50	36.3	22.7	>50	>50	>50
ETR[a]	7.48	0.496	0.277	12.0	41.3	
RPV[a]	9.11	0.335	0.346	3.41		2.17
Reference drugs	0.0590[b]	1.11[c]	0.555[d]	0.0370[e]	0.0580[f]	0.0330[g]

[a]The data of ETR and RPV were obtained from Ref. 9.
[b]Phenacetin.
[c]Mephenytoin.
[d]Tolbutamide.
[e]Dextromethorphan.
[f]Midazolam and.
[g]Testosterone were selected as reference drugs.
[h]Potential inhibition: $IC_{50} < 1$ μmol/L (high); 1 μmol/L $< IC_{50} < 10$ μmol/L (intermediate); $IC_{50} > 10$ μmol/L (low).

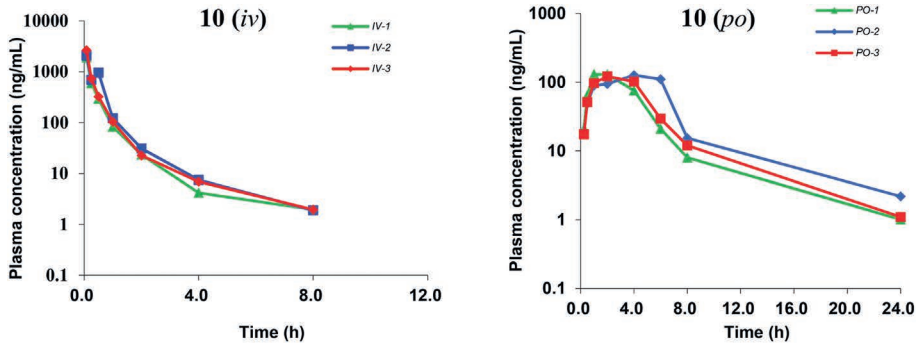

Figure 8 Plasma concentration−time curve of **10** after a dose of iv (1.0 mg/kg) and *po* (10.0 mg/kg) administration in SD rats.

Table 6 PK profiles of **10.**

Parameter	1.0 mg/kg (iv)	10.0 mg/kg (*po*)
$t_{1/2}$ (h)	1.43 ± 0.40	4.14 ± 0.35
T_{max} (h)	0.08 ± 0.00	2.33 ± 1.53
C_{max} (ng/mL)	2215 ± 386	126 ± 4
AUC_{0-t} (h·ng/mL)	918 ± 176	704 ± 139
$AUC_{0-\infty}$ (h·ng/mL)	922 ± 177	713 ± 142
MRT_{0-t} (h)	0.45 ± 0.05	4.19 ± 0.27
$MRT_{0-\infty}$ (h)	0.49 ± 0.04	4.49 ± 0.70
CL (mL/h/kg)	1114 ± 229	
F (%)		7.67 ± 1.51

and its $AUC_{0-\infty}$ was about 713 h ng/mL. Ultimately, the oral bioavailability (*F*) of **10** was calculated to be 7.67%, which surpassed that of ETR (undetectable).

3. Conclusions

In summary, aiming to alleviate cardiac toxicity and enhance selectivity, a series of novel furo-[3,2-*d*]pyrimidine derivatives featuring the aminopiperidine ring or modified *p*-cyanoaniline moiety on the right wing as well as biphenyl fragment on the left wing were rationally designed *via* scaffold hopping strategy. At the first round, we had exploited diverse chains and sizes of hydrogen acceptors/donators to protrude to the tolerant-regions I to explore their effects on antiviral activity. It was found that the introduction of hydrophilic groups on the terminal was beneficial to the antiviral activity while lipophilic groups were deleterious as expected. Although many derivatives displayed exceptional inhibitory activity against WT strain, they exhibited significantly reduced potency against the RES056 strain and were associated with high cytotoxicity. Consequently, the more flexible and metabolism-susceptible piperidine moiety containing a basic aliphatic amine, generally recognized as hERG pharmacophore, was replaced with modified *p*-cyanoaniline group of RPV by adding fluorine or nitrogen atom on the second round. Notably, compound **10** demonstrated to be most potent inhibitor against various HIV-1 strains (EC_{50} = 1.9−46.3 nmol/L), more potent than EFV (EC_{50} = 4.1−393.6 nmol/L), comparable to ETR (EC_{50} = 3.1−23.9 nmol/L) and RPV (EC_{50} = 1.0−81.6 nmol/L). It was particularly noticeable that **10** exhibited exceedingly improved inhibitory potency towards Y188L (EC_{50} = 15.5 nmol/L) and F227L + V106A (EC_{50} = 8.7 nmol/L) strain, which were 5.1- and 9.4-fold more potent than RPV ($EC_{50\ (Y188L)}$ = 79.4 nmol/L, $EC_{50\ (F227L\ +\ V106A)}$ = 81.6 nmol/L), respectively. More encouragingly, **10** displayed negligible cytotoxicity (CC_{50} = 314.8 μmol/L) and high selectivity index (SI = 161,580). **10** demonstrated high affinity for WT HIV-1 RT (IC_{50} = 50 nmol/L) as a classical NNRTI. More importantly, no apparent inhibition of the hERG potassium channel (IC_{50} > 30 μmol/L) was observed, as well as six CYP enzymes. The pharmacokinetic evaluation demonstrated extended half-life time and favorable plasma exposure compared to NNRTI. Overall, these findings illustrated that **10** was a potentially promising NNRTI for HIV-1 therapy.

4. Experimental

4.1. Chemistry

Chemical reagents and solvents obtained from commercial sources were utilized without purification unless specifically noted. Melting points were measured on a micromelting point apparatus or an automatic melting point apparatus (MP450) without correction. ^{1}H NMR, ^{13}C NMR, and ^{19}F NMR spectra were recorded on a Bruker AV-400 spectrometer (Bruker BioSpin, Fallanden, Switzerland). Chemical shifts were expressed as δ units (ppm) and *J* values were presented in hertz (Hz) using tetramethylsilane (TMS) as an internal standard. Signals were abbreviated as s (singlet), d (doublet), t (triplet), q (quartet) or m (multiplet), ect. High-resolution mass spectrometry (HRMS) was carried out on a Waters Quattro Micromass and Bruker SolariX-70 FT-MS with electrospray ionization (ESI). Thin-layer chromatography (TLC) was performed on silica gel GF254, column chromatography with 200−300 mesh silica gel and spots were visualized by irradiation with UV light (λ = 254 nm). Concentration of solutions was conducted on rotary evaporator under reduced pressure.

4.1.1. General procedure of the preparation of the intermediate *4*

A reaction mixture of prepared diphenol (10.58 mmol, 1.0 eq) and K_2CO_3 (21.0 mmol, 2.2 eq) in anhydrous DMF (50 mL) was stirred at room temperature for 20 min. Compound **3** (10.58 mmol, 1.0 eq) was subsequently added and the mixture was continued to stir for extra 2 h until completion of reaction detected by TLC analysis. The mixture was then poured into water (200 mL) resulting in a substantial amount of precipitate. The white precipitate was collected by filtration, rinsed with a small quantity of cold ethanol and dried under vacuum oven to obtain compound **4** as a white solid (yield: 90%). ^{1}H NMR (400 MHz, $CDCl_3$) δ 8.00

(d, J = 2.2 Hz, 1H), 7.72 (d, J = 8.3 Hz, 2H), 7.68 (d, J = 8.3 Hz, 2H), 7.33 (s, 2H), 6.98 (d, J = 2.2 Hz, 1H), 2.22 (s, 6H). ^{13}C NMR (101 MHz, $CDCl_3$) δ 156.8, 153.9, 153.2, 152.3, 149.5, 145.0, 137.3, 133.1, 132.6, 131.4, 127.9, 127.8, 119.0, 111.0, 107.9, 16.8. HRMS Calcd. for $C_{21}H_{15}ClN_3O_2$ $[M + H]^+$: 376.0847, found 376.0847.

*4.1.2. General procedure of the preparation of the intermediate **5***

To a bottle of 50 mL were added *N*-Boc-4-aminopiperidine (42.0 mmol, 5.0 eq) and compound **4** (8.3 mmol, 1.0 eq), the mixture was degassed and purged with N_2 for three times. After heated to 120 °C for 12 h and monitored to completion by TLC, the reaction mixture was cooled to rt, dissolved in 40 mL of ethyl acetate and poured into water (100 mL). The organic layer was extracted, dried over Na_2SO_4, and purified by column chromatography on silica gel, eluting with petroleum ether/ethyl acetate to afford compound **5** as a pale yellow foamy solid (yield: 74%). ^{1}H NMR (400 MHz, $CDCl_3$) δ 7.76 (d, J = 2.2 Hz, 1H), 7.72 (d, J = 8.5 Hz, 2H), 7.68 (d, J = 8.5 Hz, 2H), 7.32 (s, 2H), 6.70 (d, J = 2.2 Hz, 1H), 4.72 (d, J = 7.3 Hz, 1H), 4.02−3.56 (m, 3H), 2.82−2.62 (m, 2H), 2.22 (s, 6H), 1.93−1.84 (m, 2H), 1.42 (s, 9H), 1.30−1.18 (m, 2H). ^{13}C NMR (101 MHz, $CDCl_3$) δ 158.6, 156.3, 154.8, 153.0, 150.6, 150.1, 145.1, 136.6, 132.7, 131.9, 129.0, 127.6, 127.4, 119.0, 110.8, 107.0, 79.6, 49.0, 42.6, 32.0, 28.5, 16.8. HRMS Calcd. for $C_{31}H_{34}N_5O_4$ $[M + H]^+$: 540.2605, found 540.2609.

*4.1.3. General procedure of the preparation of the intermediate **6***

To a solution of compound **5** (2.8 mmol, 1.0 eq) in CH_2Cl_2 (5 mL) was added TFA (28.0 mmol, 10.0 eq) and the reaction was stirred at 25 °C for 4 h (monitored by TLC). The mixture was quenched by the addition of sat. $NaHCO_3$ to make pH 7−8, followed by stirring at rt for 2 h. The precipitated pale-yellow solid was collected by filtration, washed with water and a small amount of cold ethanol, and dried to afford **6** without further separation (yield: 88%). HRMS Calcd. for $C_{26}H_{26}N_5O_2$ $[M + H]^+$: 440.2081, found 440.2079.

*4.1.4. General procedure of the preparation of the targeted compounds **7a−z** and **7aa−af***

A mixture of compound **6** (0.25 mmol, 1.0 eq), diverse substituted benzyl bromide or chloride (0.3 mmol, 1.2 eq) and K_2CO_3 (0.5 mmol, 2.0 eq) in DMF (2 mL) was stirred at rt for 12 h. Upon completion, the reaction mixture was poured into water (100 mL) and the resulting precipitate was collected by filtration. The crude product was purified by column chromatography on silica gel using CH_2Cl_2/MeOH as the eluent. The elution was concentrated and dried to gain the desired products **7a−z** and **7aa−af** (yield: 22%−77%).

*4.1.5. General procedure of the preparation of the targeted compounds **8−10***

To a mixture of intermediate **4** (0.5 mmol, 1.0 eq), different aromatic amine (0.5 mmol, 1.0 eq), Cs_2CO_3 (1.0 mmol, 2.0 eq) in dioxane (6 mL) were treated with $Pd_2(dba)_3$ (5% mol), BINAP (10% mol). The reaction was degassed and purged with N_2 gas for three times and stirred at 100 °C for 12 h. Upon completion, the reaction mixture was cooled to rt, diluted with EtOAc, and filtered. The filtrate was washed with water, saturated NaCl solution and dried over anhydrous Na_2SO_4, followed by concentration and further purification by silica gel chromatography (EA/PE) to afford **9** (yield: 89%) or **10** (yield: 87%) as off-white solid. Targeted compounds **8** (yield: 92%) was obtained following the similar procedure.

*4-((4-((4-((4′-Cyano-3,5-dimethyl-[1,1′-biphenyl]-4-yl)oxy)furo[3,2-d]pyrimidin-2-yl)amino)piperidin-1-yl)methyl)benzenesulfonamide (**7a**).* White solid, yield: 54%, mp: 152.9−154.0 °C. ^{1}H NMR (400 MHz, DMSO-d_6) δ 8.20 (d, J = 2.2 Hz, 1H, furan-H), 7.95 (d, J = 8.0 Hz, 2H, PhH), 7.90 (d, J = 8.0 Hz, 2H, PhH), 7.75 (d, J = 7.8 Hz, 2H, PhH), 7.56 (s, 2H, PhH), 7.49−7.33 (m, 2H, PhH), 7.31 (s, 2H, SO_2NH_2), 6.86 (s, 1H, furan-H), 6.73 (br., 1H, NH), 3.74−3.37 (m, 3H, Ph-CH_2-N-, NH-C<u>H</u>-), 2.85−2.57 (m, 2H, -N(C<u>H</u>$_2$C<u>H</u>$_2$)$_2$-), 2.15 (s, 6H, diCH_3), 2.05−1.13 (m, 6H, N(C<u>H</u>$_2$C<u>H</u>$_2$)$_2$). ^{13}C NMR (101 MHz, DMSO-d_6) δ 159.1, 156.8, 152.7, 152.5, 150.2, 144.7, 143.3, 143.2, 136.2, 133.4, 131.9, 129.5, 128.0, 127.8, 126.1, 119.5, 110.4, 107.3, 62.0, 52.9, 49.1, 31.7, 16.8. HRMS Calcd. for $C_{33}H_{33}N_6O_4S$ $[M + H]^+$: 609.2279, found 609.2262.

*4-((4-((4-((4′-Cyano-3,5-dimethyl-[1,1′-biphenyl]-4-yl)oxy)furo[3,2-d]pyrimidin-2-yl)amino)piperidin-1-yl)methyl)-N-methylbenzenesulfonamide (**7b**).* White solid, yield: 49%, mp: 242.8−244.8 °C. ^{1}H NMR (400 MHz, $CDCl_3$) δ 7.80 (d, J = 7.9 Hz, 2H, PhH), 7.77−7.67 (m, 5H, PhH, furan-H), 7.47 (d, J = 7.7 Hz, 2H, PhH), 7.33 (s, 2H, PhH), 6.69 (d, J = 2.2 Hz, 1H, furan-H), 4.78 (s, 1H, NH), 4.65 (s, 1H, SO_2NH), 3.76-3.37 (m, 3H), 2.90−2.70 (m, 2H), 2.66 (d, J = 5.4 Hz, 3H, -SO_2NHC<u>H</u>$_3$), 2.22 (s, 6H, diMe), 2.15−1.40 (m, 6H). ^{13}C NMR (101 MHz, $CDCl_3$) δ 158.7, 156.3, 153.0, 150.6, 150.2, 145.2, 137.9, 136.5, 132.6, 131.9, 129.8, 128.9, 127.7, 127.3, 119.0, 110.8, 106.9, 62.1, 52.2, 48.4, 31.6, 29.3, 16.8. HRMS Calcd. for $C_{34}H_{35}N_6O_4S$ $[M + H]^+$: 623.2435, found 623.2435.

*3′,5′-Dimethyl-4′-((2-((1-(4-(methylsulfonyl)benzyl)piperidin-4-yl)amino)furo[3,2-d]pyrimidin-4-yl)oxy)-[1,1′-biphenyl]-4-carbonitrile (**7c**).* White solid, yield: 69%, mp: 136.5−137.9 °C. ^{1}H NMR (400 MHz, $CDCl_3$) δ 7.86 (d, J = 7.9 Hz, 2H, PhH), 7.79−7.65 (m, 5H, Ph-4H, furan-H), 7.50 (d, J = 7.9 Hz, 2H, PhH), 7.32 (s, 2H, PhH), 6.70 (d, J = 2.2 Hz, 1H, furan-H), 4.74 (d, J = 7.4 Hz, 1H, NH), 3.72−3.34 (m, 3H), 3.05 (s, 3H, SO_2CH_3), 2.83−2.65 (m, 2H), 2.22 (s, 6H, diMe), 2.16−1.80 (m, 4H), 1.55−1.34 (m, 2H). ^{13}C NMR (101 MHz, $CDCl_3$) δ 158.7, 156.3, 152.9, 150.5, 150.1, 145.1, 144.9, 139.3, 136.4, 132.6, 131.9, 129.7, 128.8, 127.6, 127.4, 127.3, 119.0, 110.7, 107.0, 62.2, 52.3, 48.5, 44.5, 31.9, 16.8. HRMS Calcd. for $C_{34}H_{34}N_5O_4S$ $[M+H]^+$: 608.2326, found 608.2315.

*4-((4-((4-((4′-Cyano-3,5-dimethyl-[1,1′-biphenyl]-4-yl)oxy)furo[3,2-d]pyrimidin-2-yl)amino)piperidin-1-yl)methyl)benzamide (**7d**).* White solid, yield: 50%, mp: 206.7−208.2 °C. ^{1}H NMR (400 MHz, DMSO-d_6) δ 8.20 (d, J = 2.2 Hz, 1H, furan-H), 8.00−7.85 (m, 5H, PhH, -CONH), 7.79 (d, J = 7.8 Hz, 2H, PhH), 7.56 (s, 2H, PhH), 7.42−7.11 (m, 3H, -ONH, PhH), 6.86 (s, 1H, furan-H), 6.73 (brs, 1H, NH), 3.83−3.37 (m, 3H), 2.83−2.58 (m, 2H), 2.14 (s, 6H, diMe), 2.05−1.15 (m, 6H). ^{13}C NMR (101 MHz, DMSO-d_6) δ 168.3, 159.1, 152.7, 152.4, 150.2, 144.6, 142.4, 136.1, 133.4, 133.3, 131.8, 128.9, 127.9, 127.9, 127.8, 119.4, 110.4, 107.3, 62.2, 52.8, 31.7, 16.8. HRMS Calcd. for $C_{34}H_{33}N_6O_3$ $[M + H]^+$: 573.2609, found 573.2600.

*4-((4-((4-((4′-Cyano-3,5-dimethyl-[1,1′-biphenyl]-4-yl)oxy)furo[3,2-d]pyrimidin-2-yl)amino)piperidin-1-yl)methyl)-N-methylbenzamide (**7e**).* White solid, yield: 72%, mp: 239.2−240.9 °C. ^{1}H NMR (400 MHz, $CDCl_3$) δ 7.84−7.61 (m, 7H, PhH), 7.38−7.26 (m, 4H, PhH), 6.69 (s, 1H, CONHCH$_3$), 6.48 (d, J = 5.7 Hz, 1H, furan-H), 4.79 (d, J = 7.3 Hz, 1H, NH), 3.75−3.27 (m, 3H), 2.98 (d, J = 4.6 Hz, 3H, CONHC<u>H</u>$_3$),

2.82−2.61 (m, 2H), 2.22 (s, 6H, diMe), 2.15−1.77 (m, 4H), 1.52−1.28 (m, 2H). ^{13}C NMR (101 MHz, $CDCl_3$) δ 167.9, 158.6, 156.1, 152.8, 150.4, 150.0, 145.0, 141.5, 136.3, 133.4, 132.4, 131.8, 128.9, 128.7, 127.4, 127.1, 126.7, 118.9, 110.5, 106.8, 62.3, 52.1, 48.5, 31.7, 26.7, 16.6. HRMS Calcd. for $C_{35}H_{35}N_6O_3$ [M + H]$^+$: 586.2765, found 587.2764.

*4′-((2-((1-(4-(Hydroxymethyl)benzyl)piperidin-4-yl)amino)furo[3,2-d]pyrimidin-4-yl)oxy)-3′,5′-dimethyl-[1,1′-biphenyl]-4-carbonitrile (**7f**).* White solid, yield: 41%, mp: 182.1−183.0 °C. ^{1}H NMR (400 MHz, $CDCl_3$) δ 7.77−7.65 (m, 5H, furan-H, PhH), 7.35−7.20 (m, 6H, PhH), 6.68 (d, J = 2.2 Hz, 1H, furan-H), 4.76 (d, J = 7.3 Hz, 1H, NH), 4.65 (s, 2H, -C$\underline{H}_2$OH), 3.64−3.24 (m, 3H), 2.80−2.65 (m, 2H), 2.26 (brs, 1H, -CH$_2$O$\underline{H}$), 2.21 (s, 6H, di-Me), 2.13−1.73 (m, 4H), 1.48−1.34 (m, 2H).$^{13}\underline{C}$ NMR (101 MHz, $CDCl_3$) δ 158.8, 156.3, 153.0, 150.5, 150.2, 145.3, 140.1, 137.2, 136.6, 132.6, 132.0, 129.5, 128.9, 127.7, 127.4, 127.0, 119.1, 110.8, 107.0, 65.0, 62.7, 52.2, 48.8, 31.9, 16.8. HRMS Calcd. for $C_{34}H_{34}N_5O_3$ [M + H]$^+$: 560.2656, found 560.2655.

*4′-((2-((1-(4-Acetylbenzyl)piperidin-4-yl)amino)furo[3,2-d]pyrimidin-4-yl)oxy)-3′,5′-dimethyl-[1,1′-biphenyl]-4-carbonitrile (**7g**).* White solid, yield: 44%, mp: 214.5−216.5 °C. ^{1}H NMR (400 MHz, $CDCl_3$) δ 7.90 (d, J = 7.9 Hz, 2H, PhH), 7.81−7.60 (m, 5H, furan-H, PhH), 7.40 (d, J = 7.9 Hz, 2H, PhH), 7.32 (s, 2H, PhH), 6.70 (d, J = 2.2 Hz, 1H, furan-H), 4.73 (d, J = 7.4 Hz, 1H, NH), 3.77−3.38 (m, 3H), 2.92−2.66 (m, 2H), 2.59 (s, 3H, $COCH_3$), 2.22 (s, 6H, diMe), 2.08−1.37 (m, 6H). ^{13}C NMR (101 MHz, $CDCl_3$) δ 197.8, 158.7, 156.3, 152.9, 150.5, 150.1, 145.2, 143.3, 136.5, 136.3, 132.6, 131.9, 129.2, 128.8, 128.4, 127.6, 127.3, 119.0, 110.7, 107.0, 62.4, 52.3, 52.3, 48.5, 31.7, 26.6, 16.8. HRMS Calcd. for $C_{33}H_{32}N_6O_4S$ [M + H]$^+$: 576.2656, found 576.2653.

*Methyl 4-((4-((4-((4′-Cyano-3,5-dimethyl-[1,1′-biphenyl]-4-yl)oxy)furo[3,2-d]pyrimidin-*2-yl*)amino)piperidin-1-yl)methyl)benzoate (**7h**).* White solid, yield: 77%, mp: 244.8−246.2 °C. ^{1}H NMR (400 MHz, $CDCl_3$) δ 7.97 (d, J = 7.9 Hz, 2H, PhH), 7.79−7.59 (m, 5H, furan-H, PhH), 7.42−7.33 (m, 2H, PhH), 7.32 (s, 2H, PhH), 6.70 (d, J = 2.2 Hz, 1H, furan-H), 4.72 (d, J = 7.4 Hz, 1H, NH), 3.91 (s, 3H, −COOMe), 3.68−3.34 (m, 3H), 2.88−2.62 (m, 2H), 2.22 (s, 6H, diMe), 2.09−1.34 (m, 6H). ^{13}C NMR (101 MHz, $CDCl_3$) δ 167.0, 158.8, 156.4, 153.0, 150.5, 150.2, 145.3, 136.6, 132.7, 132.0, 129.7, 128.9, 128.0, 127.7, 127.4, 119.0, 110.9, 107.0, 62.6, 52.4, 52.2, 48.6, 31.9, 16.8. HRMS Calcd. for $C_{35}H_{34}N_5O_4$ [M + H]$^+$: 588.2605, found 588.2603.

*3′,5′-Dimethyl-4′-((2-((1-(4-nitrobenzyl)piperidin-4-yl)amino)furo[3,2-d]pyrimidin-4-yl)oxy)-[1,1′-biphenyl]-4-carbonitrile (**7i**).* Yellow solid, yield: 69%, mp: 201.2−203.2 °C. ^{1}H NMR (400 MHz, $CDCl_3$) δ 8.15 (d, J = 8.3 Hz, 2H, PhH), 7.75 (d, J = 2.2 Hz, 1H, furan-H), 7.73 (d, J = 8.7 Hz, 2H, PhH), 7.70 (d, J = 8.5 Hz, 2H, PhH), 7.46 (d, J = 8.3 Hz, 2H, PhH), 7.33 (s, 2H, PhH), 6.70 (d, J = 2.2 Hz, 1H, furan-H), 4.74 (d, J = 7.4 Hz, 1H, NH), 3.71−3.43 (m, 3H), 2.83−2.64 (m, 2H), 2.22 (s, 6H, diMe), 2.18−1.81 (m, 4H), 1.55−1.37 (m, 2H). ^{13}C NMR (101 MHz, $CDCl_3$) δ 158.7, 156.3, 152.9, 150.5, 150.1, 147.1, 146.7, 145.1, 136.5, 132.6, 131.9, 129.3, 128.8, 127.6, 127.3, 123.5, 118.9, 110.8, 107.0, 62.2, 52.4, 48.6, 32.1, 16.8. HRMS Calcd. for $C_{33}H_{31}N_6O_4$ [M + H]$^+$: 575.2401, found 609. 575.2401.

*3′,5′-Dimethyl-4′-((2-((1-(4-(trifluoromethyl)benzyl)piperidin-4-yl)amino)furo[3,2-d]pyrimidin-4-yl)oxy)-[1,1′-biphenyl]-4-carbonitrile (**7j**).* White solid, yield: 65%, mp: 203.2−205.1 °C. ^{19}F NMR (376 MHz, $CDCl_3$) δ −62.36. ^{1}H NMR (400 MHz, $CDCl_3$) δ 7.75 (d, J = 2.2 Hz, 1H, furan-H), 7.72 (dd, J = 8.4, 2.4 Hz, 4H, PhH), 7.54 (d, J = 8.0 Hz, 2H, PhH), 7.39 (d, J = 8.0 Hz, 2H, PhH), 7.32 (s, 2H, PhH), 6.70 (d, J = 2.2 Hz, 1H, furan-H), 4.75 (d, J = 7.4 Hz, 1H, NH), 3.75−3.28 (m, 3H), 2.83−2.62 (m, 2H), 2.22 (s, 6H, diMe), 2.13−1.77 (m, 4H), 1.53−1.34 (m, 2H). ^{13}C NMR (101 MHz, $CDCl_3$) δ 158.8, 156.3, 153.0, 150.5, 150.2, 145.2, 142.4, 136.5, 132.6, 132.0, 129.8 (d, J_{C-F} = 33.0 Hz), 129.2, 128.9, 127.6, 127.3, 125.28 (q, J_{C-F} = 3.7 Hz), 124.31 (q, J_{C-F} = 271.9 Hz), 110.8, 107.0, 62.4, 52.3, 48.7, 31.9, 16.8. HRMS Calcd. for $C_{34}H_{31}F_3N_5O_2$ [M + H]$^+$: 598.2424, found 598.2422.

*4′-((2-((1-(4-Bromobenzyl)piperidin-4-yl)amino)furo[3,2-d]pyrimidin-4-yl)oxy)-3′,5′-dimethyl-[1,1′-biphenyl]-4-carbonitrile (**7k**).* White solid, yield: 64%, mp: 202.8−205.2 °C. ^{1}H NMR (400 MHz, $CDCl_3$) δ 7.80−7.63 (m, 5H, furan-H, PhH), 7.40 (d, J = 8.0 Hz, 2H, PhH), 7.32 (s, 2H, PhH), 7.14 (d, J = 8.0 Hz, 2H, PhH), 6.69 (d, J = 2.0 Hz, 1H, furan-H), 4.74 (d, J = 7.3 Hz, 1H, NH), 3.71−3.17 (m, 3H), 2.84−2.63 (m, 2H), 2.21 (s, 6H, diMe), 2.11−1.79 (m, 4H), 1.55−1.34 (m, 2H). ^{13}C NMR (101 MHz, $CDCl_3$) δ 158.8, 156.3, 153.0, 150.5, 150.2, 145.2, 136.9, 136.5, 132.6, 132.0, 131.4, 130.8, 128.9, 127.6, 127.3, 121.1, 119.0, 110.8, 107.0, 62.2, 52.2, 48.6, 31.8, 16.8. HRMS Calcd. for $C_{33}H_{31}BrN_5O_2$ [M + H]$^+$: 608.1656, found 608.1649.

*4′-((2-((1-(4-Chlorobenzyl)piperidin-4-yl)amino)furo[3,2-d]pyrimidin-4-yl)oxy)-3′,5′-dimethyl-[1,1′-biphenyl]-4-carbonitrile (**7l**).* White solid, yield: 44%, mp: 190.1−192.4 °C. ^{1}H NMR (400 MHz, $CDCl_3$) δ 7.78−7.64 (m, 5H, furan-H, PhH), 7.32 (s, 2H, PhH), 7.29−7.17 (m, 4H, PhH), 6.70 (d, J = 2.2 Hz, 1H, furan-H), 4.73 (d, J = 7.4 Hz, 1H, NH), 3.72−3.27 (m, 3H), 2.85−2.64 (m, 2H), 2.22 (s, 6H, diMe), 2.11−1.79 (m, 4H), 1.57−1.34 (m, 2H). ^{13}C NMR (101 MHz, $CDCl_3$) δ 158.8, 156.3, 153.0, 150.5, 150.2, 145.2, 136.5, 136.2, 133.0, 132.6, 132.0, 130.5, 128.9, 128.5, 127.6, 127.3, 119.0, 110.8, 107.0, 62.1, 52.1, 48.6, 31.8, 16.8. HRMS Calcd. for $C_{33}H_{31}ClN_5O_2$ [M + H]$^+$: 564.2161, found 564.2157.

*3′,5′-Dimethyl-4′-((2-((1-(4-methylbenzyl)piperidin-4-yl)amino)furo[3,2-d]pyrimidin-4-yl)oxy)-[1,1′-biphenyl]-4-carbonitrile (**7m**).* White solid, yield: 24%, mp: 212.2−213.8 °C. ^{1}H NMR (400 MHz, $CDCl_3$) δ 7.79−7.66 (m, 5H, furan-H), 7.32 (s, 2H, PhH), 7.17 (d, J = 7.6 Hz, 2H, PhH), 7.11 (d, J = 7.6 Hz, 2H, PhH), 6.69 (d, J = 2.2 Hz, 1H, furan-H), 4.74 (d, J = 7.3 Hz, 1H, NH), 3.76−3.28 (m, 3H), 2.98−2.71 (m, 2H), 2.33 (s, 3H, CH_3), 2.21 (s, 6H, diMe), 2.15−1.81 (m, 4H), 1.64−1.43 (m, 2H). ^{13}C NMR (101 MHz, $CDCl_3$) δ 158.8, 156.3, 153.0, 150.5, 150.2, 145.3, 143.8, 136.6, 132.6, 132.0, 129.6, 129.2, 129.0, 127.7, 127.4, 119.1, 110.8, 107.0, 62.5, 52.0, 48.4, 31.5, 21.2, 16.8. HRMS Calcd. for $C_{34}H_{34}N_5O_2$ [M + H]$^+$: 544.2707, found 544.2700.

*4′-((2-((1-(4-Cyanobenzyl)piperidin-4-yl)amino)furo[3,2-d]pyrimidin-4-yl)oxy)-3′,5′-dimethyl-[1,1′-biphenyl]-4-carbonitrile (**7aa**).* White solid, yield: 46%, mp: 214.5−216.5 °C. ^{1}H NMR (400 MHz, $CDCl_3$) δ 7.82−7.65 (m, 5H, furan-H, PhH), 7.59 (d, J = 7.7 Hz, 2H, PhH), 7.51−7.38 (m, 2H, PhH), 7.33 (s, 2H, PhH), 6.70 (s, 1H, furan-H), 4.73 (d, J = 7.3 Hz, 1H, NH), 3.81−3.31 (m, 3H), 2.94−2.63 (m, 2H), 2.22 (s, 6H, diMe), 2.15−1.23 (m, 6H). ^{13}C NMR (101 MHz, $CDCl_3$) δ 158.7, 156.3, 153.0, 150.5, 150.2, 145.2, 143.9, 136.5, 132.6, 132.2, 132.0, 129.5, 128.9, 127.6, 127.3, 119.0, 118.9, 111.0, 110.8, 107.0, 62.4, 52.4, 48.5, 31.9, 16.8. HRMS Calcd. for $C_{34}H_{31}N_6O_2$ [M + H]$^+$: 555.2503, found 555. 2499.

4′-((2-((1-(3-Cyanobenzyl)piperidin-4-yl)amino)furo[3,2-d]pyrimidin-4-yl)oxy)-3′,5′-dimethyl-[1,1′-biphenyl]-4-carbonitrile

*(**7 ab**)*. White solid, yield: 60%, mp: 227.1−229.2 °C. ^{1}H NMR (400 MHz, $CDCl_3$) δ 7.78−7.68 (m, 5H, furan-H, PhH), 7.60 (s, 1H, PhH), 7.56−7.47 (m, 2H, PhH), 7.40 (t, J = 7.7 Hz, 1H), 7.33 (s, 2H, PhH), 6.71 (s, 1H, furan-H), 4.73 (d, J = 7.4 Hz, 1H, NH), 3.66−3.33 (m, 3H), 2.82−2.64 (m, 2H), 2.22 (s, 6H, diMe), 2.14−1.40 (m, 6H). ^{13}C NMR (101 MHz, $CDCl_3$) δ 158.7, 156.3, 153.0, 150.5, 150.2, 145.2, 140.1, 136.5, 133.3, 132.6, 132.3, 131.9, 130.8, 129.1, 128.9, 127.6, 127.3, 119.0, 112.4, 110.8, 107.0, 62.0, 52.3, 48.6, 31.9, 16.8. HRMS Calcd. for $C_{34}H_{31}N_6O_2$ $[M + H]^+$: 555.2503, found 555.2499.

*4′-((2-((1-(2-Cyanobenzyl)piperidin-4-yl)amino)furo[3,2-d] pyrimidin-4-yl)oxy)-3′,5′-dimethyl-[1,1′-biphenyl]-4-carbonitrile (**7ac**)*. White solid, yield: 62%, mp: 205.1−206.3 °C. ^{1}H NMR (400 MHz, $CDCl_3$) δ 7.76 (d, J = 2.2 Hz, 1H, furan-H), 7.71 (dd, J = 8.5, 2.1 Hz, 4H, PhH), 7.62 (d, J = 7.7 Hz, 1H, PhH), 7.54 (t, J = 7.3 Hz, 2H, PhH), 7.36 (d, J = 8.0 Hz, 1H, PhH), 7.33 (s, 2H, PhH), 6.70 (d, J = 2.2 Hz, 1H, furan-H), 4.74 (d, J = 7.1 Hz, 1H, NH), 3.97−3.35 (m, 3H), 2.95−2.67 (m, 2H), 2.22 (s, 6H, diMe), 2.20−1.75 (m, 4H), 1.60−1.36 (m, 2H). ^{13}C NMR (101 MHz, $CDCl_3$) δ 158.8, 156.3, 152.9, 150.5, 150.1, 145.2, 142.4, 136.5, 132.9, 132.66, 132.63, 131.9, 130.0, 128.8, 127.66, 127.63, 127.3, 119.0, 117.8, 112.9, 110.8, 107.0, 60.4, 52.2, 48.7, 31.9, 16.8. HRMS Calcd. for $C_{34}H_{31}N_6O_2$ $[M + H]^+$: 555.2503, found 555.2504.

*3′,5′-Dimethyl-4′-((2-((1-(pyridin-4-ylmethyl)piperidin-4-yl) amino)furo[3,2-d]pyrimidin-4-yl)oxy)-[1,1′-biphenyl]-4-carbonitrile (**7ad**)*. Brown solid, yield: 62%, mp: 203.0−205.5 °C. ^{1}H NMR (400 MHz, $CDCl_3$) δ 8.54 (s, 2H, PyH), 7.82−7.58 (m, 5H, furan-H, PhH), 7.32 (s, 2H, PhH), 7.26 (s, 2H, PyH), 6.70 (s, 1H, furan-H), 4.77 (d, J = 7.2 Hz, 1H, NH), 3.72−3.27 (m, 3H), 2.94−2.66 (m, 2H), 2.21 (s, 6H, diMe), 2.16−1.79 (m, 4H), 1.66−1.44 (m, 2H). ^{13}C NMR (101 MHz, $CDCl_3$) δ 158.7, 156.3, 153.0, 150.6, 150.1, 149.9, 146.5, 145.2, 136.5, 132.6, 131.9, 128.9, 127.6, 127.3, 124.1, 119.0, 110.8, 107.0, 61.5, 52.3, 48.3, 31.5, 16.8. HRMS Calcd. for $C_{32}H_{31}N_6O_2$ $[M + H]^+$: 531.2503, found 531.2493.

*3′,5′-Dimethyl-4′-((2-((1-(pyridin-3-ylmethyl)piperidin-4-yl) amino)furo[3,2-d]pyrimidin-4-yl)oxy)-[1,1′-biphenyl]-4-carbonitrile (**7ae**)*. Brown solid, yield: 49%, mp: 201.5−203.1 °C. ^{1}H NMR (400 MHz, $CDCl_3$) δ 8.55−8.42 (m, 2H, Py-α,α'H), 7.79−7.64 (m, 6H, furan-H, PhH, Py-γH), 7.32 (s, 2H, PhH), 7.23 (dd, J = 7.8, 4.8 Hz, 1H, Py-βH), 6.69 (d, J = 2.2 Hz, 1H, furan-H), 4.75 (d, J = 7.4 Hz, 1H, NH), 3.74−3.23 (m, 3H), 2.93−2.66 (m, 2H), 2.21 (s, 6H, diMe), 2.17−1.81 (m, 4H), 1.59−1.35 (m, 2H). ^{13}C NMR (101 MHz, $CDCl_3$) δ 158.8, 156.3, 152.9, 150.5, 150.4, 150.1, 148.8, 145.2, 136.8, 136.5, 133.3, 132.6, 131.9, 128.9, 127.6, 127.3, 123.4, 119.0, 110.8, 107.0, 60.1, 52.2, 48.6, 31.8, 16.8. HRMS Calcd. for $C_{32}H_{31}N_6O_2$ $[M + H]^+$: 531.2503, found 531.2504.

*3′,5′-Dimethyl-4′-((2-((1-(pyridin-2-ylmethyl)piperidin-4-yl) amino)furo[3,2-d]pyrimidin-4-yl)oxy)-[1,1′-biphenyl]-4-carbonitrile (**7af**)*. Brown solid, yield: 39%, mp: 203.3−205.1 °C. ^{1}H NMR (400 MHz, $CDCl_3$) δ 8.53 (dd, J = 5.2, 1.8 Hz, 1H, Py-αH), 7.74 (d, J = 2.2 Hz, 1H, furan-H), 7.70 (dd, J = 8.4, 2.0 Hz, 4H, PhH), 7.61 (td, J = 7.7, 1.8 Hz, 1H, Py-γH), 7.34 (d, J = 7.9 Hz, 1H, Py-β'H), 7.31 (s, 2H, PhH), 7.14 (ddd, J = 7.5, 4.8, 1.2 Hz, 1H, Py-βH), 6.69 (d, J = 2.2 Hz, 1H, furan-H), 4.77 (d, J = 7.4 Hz, 1H, NH), 3.70−3.40 (m, 3H), 2.95−2.70 (m, 2H), 2.21 (s, 6H, diMe), 2.16−1.77 (m, 4 H), 1.52−1.39 (m, 2H). ^{13}C NMR (101 MHz, $CDCl_3$) δ 158.8, 157.8, 156.3, 153.0, 150.5, 150.1, 149.3, 145.2, 136.6, 136.5, 132.6, 131.9, 128.9, 127.7, 127.4, 123.5, 122.3, 119.0, 110.8, 107.0, 64.4, 52.5, 48.5, 31.7, 16.8. HRMS Calcd. for $C_{32}H_{31}N_6O_2$ $[M + H]^+$: 531.2503, found 531.2505.

*3′,5′-Dimethyl-4′-((2-((1-(4-(morpholine-4-carbonyl)benzyl) piperidin-4-yl)amino)furo[3,2-d]pyrimidin-4-yl)oxy)-[1,1′-biphenyl]-4-carbonitrile (**7n**)*. White solid, yield: 68%, mp: 202.8-205.1 °C. ^{1}H NMR (400 MHz, $CDCl_3$) δ 7.78−7.65 (m, 5H, PhH, furan-H), 7.37−7.28 (m, 6H, PhH), 6.69 (d, J = 2.2 Hz, 1H, furan-H), 4.75 (d, J = 7.2 Hz, 1H, NH), 3.90−3.30 (m, 11H), 2.86−2.61 (m, 2H), 2.21 (s, 6H, Di-Me), 2.14−1.77 (m, 4H), 1.55−1.34 (m, 2H). ^{13}C NMR (101 MHz, $CDCl_3$) δ 170.3, 158.7, 156.3, 152.9, 150.5, 150.1, 145.1, 140.2, 136.4, 134.1, 132.5, 131.9, 129.1, 128.8, 127.6, 127.3, 127.1, 118.9, 110.7, 106.9, 66.9, 62.5, 52.2, 48.7, 48.2, 42.5, 31.9, 16.7. HRMS Calcd. for $C_{38}H_{39}N_6O_4$ $[M + H]^+$: 643.3027, found 643.3010.

*3′,5′-Dimethyl-4′-((2-((1-(4-(thiomorpholine-4-carbonyl) benzyl)piperidin-4-yl)amino)furo[3,2-d]pyrimidin-4-yl)oxy) -[1,1′-biphenyl]-4-carbonitrile (**7o**)*. White solid, yield: 69%, mp: 154.1−155.7 °C. ^{1}H NMR (400 MHz, $CDCl_3$) δ 7.78−7.64 (m, 5H, PhH, furan-H), 7.41−7.27 (m, 6H, PhH), 6.69 (d, J = 2.2 Hz, 1H, furan-H), 4.73 (d, J = 7.4 Hz, 1H, NH), 4.17−3.87 (m, 2H, -CON(CH_2)), 3.85−3.60 (m, 2H, -CON(CH_2)), 3.61−3.28 (m, 3H), 2.88−2.44 (m, 6H, -S(CH_2)$_2$, -CH_2-N(CH_2)$_2$), 2.22 (s, 6H, diMe), 2.14−1.75 (m, 4H), 1.57−1.33 (m, 2H). ^{13}C NMR (101 MHz, $CDCl_3$) δ 170.7, 158.7, 156.3, 153.0, 150.5, 150.2, 145.2, 139.7, 136.5, 134.7, 132.6, 131.9, 129.4, 128.9, 127.6, 127.3, 126.9, 119.0, 110.8, 107.0, 62.5, 52.2, 50.2, 48.6, 44.7, 31.8, 28.1, 27.5, 16.8. HRMS Calcd. for $C_{38}H_{39}N_6O_3S$ $[M + H]^+$: 659.2799, found 659.2791.

*3′,5′-Dimethyl-4′-((2-((1-(4-(pyrrolidine-1-carbonyl)benzyl) piperidin-4-yl)amino)furo[3,2-d]pyrimidin-4-yl)oxy)-[1,1′-biphenyl]-4-carbonitrile (**7p**)*. White solid, yield: 34%, mp: 227.8−229.6 °C. ^{1}H NMR (400 MHz, $CDCl_3$) δ 7.80−7.66 (m, 5H, PhH, furan-H), 7.45 (d, J = 7.7 Hz, 2H, PhH), 7.33 (s, 2H, PhH), 7.31−7.23 (m, 2H, PhH), 6.70 (s, 1H, furan-H), 4.77 (d, J = 7.2 Hz, 1H, NH), 3.65 (t, J = 7.1 Hz, 2H, -CON(C$\underline{H}_2$C$\underline{H}_2$)$_2$), 3.57−3.33 (m, 5H, -CON(C$\underline{H}_2$C$\underline{H}_2$)$_2$, Ph-CH_2-N-, $\overline{N}$H-CH-), 2.83−2.61 (m, 2H), 2.23 (s, 6H, diMe), 2.09−1.76 (m, 8H, -CON(CH_2C$\underline{H}_2$)$_2$, -N(C$\underline{H}_2$C$\underline{H}_2$)$_2$), 1.50−1.34 (m, 2H). ^{13}C NMR (101 MHz, $\overline{C}$DCl$_3$) δ 169.6, 158.7, 156.3, 152.9, 150.5, 150.2, 145.2, 139.7, 136.4, 136.1, 132.6, 131.9, 128.9, 128.8, 127.6, 127.3, 127.1, 119.0, 110.7, 107.0, 62.6, 52.2, 49.6, 48.7, 46.2, 31.8, 26.4, 24.5, 16.8. HRMS Calcd. for $C_{38}H_{39}N_6O_3$ $[M + H]^+$: 627.3078, found 627.3067.

*4-((4-((4-((4′-Cyano-3,5-dimethyl-[1,1′-biphenyl]-4-yl)oxy) furo[3,2-d]pyrimidin-2-yl)amino)piperidin-1-yl)methyl)-N-(thiophen-2-ylmethyl)benzamide (**7q**)*. White solid, yield: 51%, mp: 135.8−137.5 °C. ^{1}H NMR (400 MHz, $CDCl_3$) δ 7.78−7.64 (m, 7H, PhH, furan-H), 7.41−7.28 (m, 4H, PhH), 7.23 (dd, J = 5.1, 1.3 Hz, 1H, thiophene-αH), 7.03 (d, J = 3.5 Hz, 1H, thiophene-β'H), 6.96 (dd, J = 5.1, 3.5 Hz, 1H, thiophene-βH), 6.69 (d, J = 2.1 Hz, 1H, furan-H), 6.55 (t, J = 5.6 Hz, 1H, -C$\underline{O}$N$\underline{H}$C$\underline{H}_2$-), 4.80 (d, J = 5.6 Hz, 2H, -CONHC$\underline{H}_2$-), 4.73 (d, J = 7.3 Hz, 1H, NH), 3.70−3.32 (m, 3H), 2.84−2.64 (m, 2H), 2.21 (s, 6H, diMe), 2.14−1.78 (m, 4H), 1.52−1.37 (m, 2H). ^{13}C NMR (101 MHz, $CDCl_3$) δ 167.0, 158.7, 156.3, 152.9, 150.5, 150.1, 145.2, 142.0, 141.0, 136.5, 133.0, 132.6, 131.9, 129.2, 128.8, 127.6, 127.3, 127.1, 126.9, 126.2, 125.3, 119.0, 110.7, 107.0, 62.5, 52.2, 48.6, 38.8, 31.8, 16.8. HRMS Calcd. for $C_{39}H_{37}N_6O_3S$ $[M + H]^+$: 669.2642, found 669.2629.

*4′-((2-((1-(4-(4-Hydroxypiperidine-1-carbonyl)benzyl)piperidin-4-yl)amino)furo[3,2-d]pyrimidin-4-yl)oxy)-3′,5′-dimethyl-[1, 1′-biphenyl]-4-carbonitrile (**7r**)*. White solid, yield: 68%, mp: 260.0−262.1 °C. ^{1}H NMR (400 MHz, $CDCl_3$) δ 7.79−7.66 (m, 5H, PhH, furan-H), 7.35−7.27 (m, 6H, PhH), 6.69 (d, J = 2.2 Hz, 1H,

furan-H), 4.74 (d, J = 7.3 Hz, 1H, NH), 4.32−4.10 (m, 1H, -CON(C$\underline{H}_2$)), 3.97 (dq, J = 8.1, 4.0 Hz, 1H, -C$\underline{H}$OH), 3.83−3.12 (m, 6H, -CON(CH$_2$)$_2$, -NCH$_2$, -NHCH), 2.86−2.65 (m, 2H), 2.22 (s, 6H, diMe), 2.13−1.33 (m, 10H). ^{13}C NMR (101 MHz, $CDCl_3$) δ 170.3, 158.7, 156.3, 152.9, 150.5, 150.1, 145.2, 139.8, 136.4, 134.9, 132.6, 131.9, 129.1, 128.8, 127.6, 127.3, 126.8, 119.0, 110.7, 106.9, 66.9, 62.6, 52.2, 48.8, 45.0, 39.5, 34.6, 34.0, 31.9, 16.8. HRMS Calcd. for $C_{39}H_{41}N_6O_4$ [M + H]$^+$: 657.3184, found 657.3176.

*4-((4-((4-((4′-Cyano-3,5-dimethyl-[1,1′-biphenyl]-4-yl)oxy) furo[3,2-d]pyrimidin-2-yl)amino)piperidin-1-yl)methyl)-N-((tetrahydrofuran-3-yl)methyl)benzamide (**7s**).* White solid, yield: 37%, mp: 203.3−204.9 °C. ^{1}H NMR (400 MHz, $CDCl_3$) δ 7.75 (d, J = 2.2 Hz, 1H, furan-H), 7.74−7.66 (m, 6H, PhH), 7.34 (d, J = 8.4 Hz, 2H, PhH), 7.31 (s, 2H, PhH), 6.69 (d, J = 2.2 Hz, 1H, furan-H), 6.51 (t, J = 5.9 Hz, 1H, -CON$\underline{H}$), 4.78 (d, J = 7.4 Hz, 1H, NH), 3.90 (td, J = 8.3, 5.3 Hz, 1H, O-C$\underline{H}_2$CH$_2$-), 3.82 (dd, J = 8.8, 6.8 Hz, 1H, O-C$\underline{H}_2$CH-), 3.73 (q, J = 7.7 Hz, 1H, -CONHC$\underline{H}_2$-), 3.63 (dd, J = 8.8, 4.9 Hz, 1H, O-C$\underline{H}_2$CH-), 3.58−3.40 (m, 5H, O-C$\underline{H}_2$CH$_2$-, -CONHC$\underline{H}_2$, Ph-C$\underline{H}_2$-N-, NH-C$\underline{H}$-), 2.84−2.68 (m, 2H), 2.60 (hept, J = 6.8 Hz, 1H, O-CH$_2$C$\underline{H}$-), 2.21 (s, 6H, diMe), 2.15−1.82 (m, 5H, O-CH$_2$C$\underline{H}_2$, N(C$\underline{H}_2$C$\underline{H}_2$)$_2$), 1.68 (dtd, J = 12.7, 7.5, 5.5 Hz, 1H, O-CH$_2$C$\underline{H}_2$), 1.56−1.40 (m, 2H). ^{13}C NMR (101 MHz, $CDCl_3$) δ 167.6, 158.7, 156.3, 152.9, 150.5, 150.1, 145.1, 141.7, 136.4, 133.4, 132.5, 131.9, 129.1, 128.8, 127.6, 127.3, 126.9, 119.0, 110.6, 106.9, 71.4, 67.8, 62.4, 52.2, 48.6, 42.9, 39.0, 31.8, 29.9, 16.7. HRMS Calcd. for $C_{39}H_{41}N_6O_4$ [M + H]$^+$: 657.3184, found 657.3160.

*3′,5′-Dimethyl-4′-((2-((1-(4-(pyrrolidin-1-ylsulfonyl)benzyl) piperidin-4-yl)amino)furo[3,2-d]pyrimidin-4-yl)oxy)-[1,1′-- biphenyl]-4-carbonitrile (**7t**).* White solid, yield: 53%, mp: 132.6−134.8 °C. ^{1}H NMR (400 MHz, $CDCl_3$) δ 7.81−7.65 (m, 7H, PhH, furan-H), 7.56−7.41 (m, 2H, PhH), 7.33 (s, 2H, PhH), 6.70 (d, J = 2.2 Hz, 1H, furan-H), 4.75 (d, J = 7.4 Hz, 1H, NH), 3.78−3.37 (m, 3H), 3.29−3.14 (m, 4H, SO$_2$N(C$\underline{H}_2$CH$_2$)$_2$), 2.91−2.69 (m, 2H), 2.22 (s, 6H, diMe), 2.02−1.85 (m, 4H, SO$_2$N(CH$_2$C$\underline{H}_2$)$_2$), 1.82−1.70 (m, 4H), 1.62−1.45 (m, 2H). ^{13}C NMR (101 MHz, $CDCl_3$) δ 158.7, 156.3, 152.9, 150.5, 150.1, 145.1, 142.9, 136.5, 135.9, 132.6, 131.9, 129.5, 128.9, 127.6, 127.6, 127.3, 119.0, 110.7, 107.0, 62.1, 52.3, 48.4, 47.9, 31.7, 25.2, 16.8. HRMS Calcd. for $C_{37}H_{39}N_6O_4S$ [M + H]$^+$: 663.2748, found 663.2730.

*4′-((2-((1-(4-((4-Hydroxypiperidin-1-yl)sulfonyl)benzyl)piperidin-4-yl)amino)furo[3,2-d]pyrimidin-4-yl)oxy) -3′,5′-dimethyl-[1,1′-biphenyl]-4-carbonitrile (**7u**).* White solid, yield: 54%, mp: 213.4−215.6 °C. ^{1}H NMR (400 MHz, $CDCl_3$) δ 7.78−7.63 (m, 7H, PhH, furan-H), 7.45 (d, J = 7.7 Hz, 2H, PhH), 7.33 (s, 2H, PhH), 6.69 (d, J = 2.2 Hz, 1H, furan-H), 4.78 (d, J = 7.4 Hz, 1H, NH), 3.82−3.72 (m, 1H, -C$\underline{H}$OH), 3.66−3.39 (m, 3H), 3.29 (ddd, J = 11.7, 7.5, 3.5 Hz, 2H, SO$_2$N(C$\underline{H}_2$CH$_2$)-), 2.89 (ddd, J = 11.7, 8.0, 3.6 Hz, 2H, SO$_2$N(C$\underline{H}_2$CH$_2$)-), 2.84−2.70 (m, 2H), 2.22 (s, 6H, diMe), 2.16−1.74 (m, 7H, SO$_2$N(CH$_2$C$\underline{H}_2$)$_2$C$\underline{H}$OH, N(C$\underline{H}_2$C$\underline{H}_2$)$_2$), 1.63 (ddt, J = 16.0, 7.6, 3.7 Hz, 2H, SO$_2$N(CH$_2$C$\underline{H}_2$)), 1.55−1.43 (m, 2H). ^{13}C NMR (101 MHz, $CDCl_3$) δ 158.7, 156.3, 153.0, 150.6, 150.2, 145.2, 143.2, 136.5, 135.2, 132.6, 132.0, 129.6, 128.9, 127.7, 127.6, 127.3, 119.0, 110.8, 106.9, 65.7, 62.2, 52.2, 48.4, 43.2, 33.2, 31.7, 16.8. HRMS Calcd. for $C_{38}H_{41}N_6O_5S$ [M + H]$^+$: 693.2854, found 693.2829.

*4-((4-((4-((4′-Cyano-3,5-dimethyl-[1,1′-biphenyl]-4-yl)oxy) furo[3,2-d]pyrimidin-2-yl)amino)piperidin-1-yl)methyl) -N-(2-hydroxyethyl)benzamide (**7v**).* White solid, yield: 54%, mp: 156.2−158.8 °C. ^{1}H NMR (400 MHz, DMSO-d_6) δ 8.38 (t, J = 5.7 Hz, 1H, CONH), 8.20 (d, J = 2.2 Hz, 1H, furan-H), 7.94 (d, J = 8.2 Hz, 2H, PhH), 7.89 (d, J = 8.4 Hz, 2H, PhH), 7.78 (d, J = 8.0 Hz, 2H, PhH), 7.56 (s, 2H, PhH), 7.40−7.15 (m, 2H, PhH), 6.86 (s, 1H, furan-H), 6.72 (brs, 1H, NH), 4.73 (t, J = 5.6 Hz, 1H, CONHC$\underline{H}_2$), 3.51 (q, J = 5.9 Hz, 2H, -C$\underline{H}_2$OH), 3.33 (q, J = 5.9 Hz, 2H, CONHC$\underline{H}_2$, OH), 2.86−2.56 (m, 2H), 2.15 (s, 6H, diMe), 2.06−1.19 (m, 6H). ^{13}C NMR (101 MHz, DMSO-d_6) δ 166.6, 159.1, 156.7, 152.6, 152.4, 150.1, 144.6, 142.3, 136.1, 133.7, 133.3, 131.8, 128.9, 127.9, 127.7, 127.5, 119.3, 110.3, 107.2, 62.2, 60.2, 52.8, 48.9, 42.6, 31.7, 16.7. HRMS Calcd. for $C_{36}H_{37}N_6O_4$ [M + H]$^+$: 617.2871, found 617.2856.

*4-((4-((4-((4′-Cyano-3,5-dimethyl-[1,1′-biphenyl]-4-yl)oxy) furo[3,2-d]pyrimidin-2-yl)amino)piperidin-1-yl)methyl) -N-(2-methoxyethyl)benzamide (**7w**).* White solid, yield: 66%, mp: 205.6−207.1 °C. ^{1}H NMR (400 MHz, $CDCl_3$) δ 7.82−7.65 (m, 7H, Ph-6H, furan-H), 7.42−7.34 (m, 2H, PhH), 7.32 (s, 2H, PhH), 6.70 (d, J = 2.1 Hz, 1H, furan-H), 6.52 (t, J = 5.0 Hz, 1H, -CON$\underline{H}$), 4.73 (d, J = 7.3 Hz, 1H, NH), 3.65 (q, J = 5.2 Hz, 2H), 3.60−3.42 (m, 5H), 3.39 (s, 3H, -OCH$_3$), 2.90−2.65 (m, 2H), 2.21 (s, 6H, diMe), 2.12−1.37 (m, 6H). ^{13}C NMR (101 MHz, $CDCl_3$) δ 167.3, 158.8, 156.3, 152.9, 150.5, 150.2, 145.2, 141.8, 136.5, 133.4, 132.6, 131.9, 129.1, 128.8, 127.6, 127.3, 127.0, 119.0, 110.7, 107.0, 71.2, 62.5, 58.8, 52.3, 48.7, 39.7, 31.9, 16.8. HRMS Calcd. for $C_{37}H_{39}N_6O_4$ [M + H]$^+$: 631.3027, found 631.3018.

*4-((4-((4-((4′-Cyano-3,5-dimethyl-[1,1′-biphenyl]-4-yl)oxy) furo[3,2-d]pyrimidin-2-yl)amino)piperidin-1-yl)methyl) -N-(3-hydroxypropyl)benzamide (**7x**).* White solid, yield: 44%, mp: 189.9−191.4 °C. ^{1}H NMR (400 MHz, $CDCl_3$) δ 7.84−7.58 (m, 7H, PhH, furan-H), 7.43−7.28 (m, 4H, PhH), 6.97 (t, J = 5.8 Hz, 1H, -CON$\underline{H}$), 6.69 (s, 1H, furan-H), 4.80 (d, J = 7.1 Hz, 1H, NH), δ 3.69 (t, J = 5.4 Hz, 2H, -C$\underline{H}_2$OH), 3.60 (q, J = 5.9 Hz, 2H, -CONHC$\underline{H}_2$), 3.56−3.40 (m, 3H, -PhC$\underline{H}_2$-N, -NHC$\underline{H}$), 2.81−2.63 (m, 2H), 2.21 (s, 6H, diMe), 2.13−1.69 (m, 6H), 1.56−1.32 (m, 2H). ^{13}C NMR (101 MHz, $CDCl_3$) δ 168.2, 158.8, 156.3, 153.0, 150.6, 150.2, 145.2, 141.3, 136.5, 133.3, 132.6, 132.0, 129.3, 128.9, 127.7, 127.4, 127.1, 119.1, 110.7, 107.0, 62.4, 59.9, 52.3, 48.6, 37.4, 32.1, 31.7, 16.8. HRMS Calcd. for $C_{37}H_{39}N_6O_4$ [M + H]$^+$: 631.3027, found 631.3012.

*4-((4-((4-((4′-Cyano-3,5-dimethyl-[1,1′-biphenyl]-4-yl)oxy) furo[3,2-d]pyrimidin-2-yl)amino)piperidin-1-yl)methyl) -N-(2-hydroxyethyl)benzenesulfonamide (**7y**).* White solid, yield: 22%, mp: 203.1−205.2 °C. ^{1}H NMR (400 MHz, $CDCl_3$) δ 7.84−7.60 (m, 7H, PhH, furan-H), 7.42 (d, J = 7.9 Hz, 2H, PhH), 7.32 (s, 2H, PhH), 6.69 (d, J = 2.2 Hz, 1H, furan-H), 5.76 (s, 1H, SO$_2$N$\underline{H}$), 4.94 (s, 1H, NH), 3.63 (t, J = 5.1 Hz, 2H, -C$\underline{H}_2$OH), 3.60−3.38 (m, 3H), 3.20−2.88 (m, 3H, -SO$_2$NHC$\underline{H}_2$-CH$_2$O$\underline{H}$), 2.86−2.63 (m, 2H), 2.21 (s, 6H, diMe), 2.16−1.74 (m, 4H), 1.61−1.34 (m, 2H). ^{13}C NMR (101 MHz, $CDCl_3$) δ 158.7, 156.3, 153.0, 150.6, 150.2, 145.2, 143.0, 138.8, 136.5, 132.7, 132.0, 129.8, 128.9, 127.6, 127.3, 127.1, 119.0, 110.8, 106.9, 62.1, 61.1, 52.3, 48.5, 45.4, 31.6, 16.8. HRMS Calcd. for $C_{35}H_{37}N_6O_5S$ [M + H]$^+$: 653.2541, found 653.2522.

*4-((4-((4-((4′-Cyano-3,5-dimethyl-[1,1′-biphenyl]-4-yl)oxy)furo[3,2-d]pyrimidin-2-yl)amino)piperidin-1-yl)methyl)-N-(2-methoxyethyl)benzenesulfonamide (**7z**).* White solid, yield: 46%, mp: 203.2−205.2 °C. ^{1}H NMR (400 MHz, $CDCl_3$) δ 7.79 (d, J = 8.0 Hz, 2H, PhH), 7.76−7.67 (m, 5H, furan-H, PhH), 7.46 (d, J = 8.0 Hz, 2H, PhH), 7.32 (s, 2H, PhH), 6.70 (d, J = 2.1 Hz, 1H, furan-H), 5.13 (s, 1H, -SO$_2$NH), 4.81 (s, 1H, NH), 3.76−3.46 (m, 3H), 3.41 (t, J = 5.0 Hz, 2H, -C$\underline{H}_2$OCH$_3$), 3.26 (s, 3H, OCH$_3$), 3.11 (dt, J = 9.6, 5.0 Hz, 2H, SO$_2$NHC$\underline{H}_2$), 2.93−2.71 (m, 2H),

2.22 (s, 6H, diMe), 2.19−1.78 (m, 4H), 1.65−1.37 (m, 2H). ^{13}C NMR (101 MHz, $CDCl_3$) δ 158.7, 156.3, 153.0, 150.6, 150.2, 145.2, 139.1, 136.5, 132.6, 132.0, 129.8, 128.9, 128.7, 127.7, 127.4, 127.2, 119.0, 110.8, 107.0, 70.8, 62.0, 58.8, 52.2, 48.2, 43.0, 31.6, 16.8. HRMS Calcd. for $C_{36}H_{39}N_6O_5S$ $[M + H]^+$: 667.2697, found 667.2688.

*4′-((2-((4-Cyano-3-fluorophenyl)amino)furo[3,2-d]pyrimidin-4-yl)oxy)-3′,5′-difluoro-[1,1′-biphenyl]-4-carbonitrile (**8**).* Off-white solid, yield: 92%, mp: >300 °C. ^{19}F NMR (376 MHz, DMSO-d_6) δ −107.02 (s, 1F), −125.47 (s, 2F). ^{1}H NMR (400 MHz, DMSO-d_6) δ 10.39 (s, 1H, NH), 8.52 (d, J = 2.3 Hz, 1H, furan-H), 8.03 (d, J = 8.2 Hz, 2H, PhH), 8.00 (d, J = 8.2 Hz, 2H, PhH), 7.92 (d, J = 9.5 Hz, 2H, PhH), 7.73 (d, J = 13.2 Hz, 1H, PhH), 7.60 (t, J = 8.2 Hz, 1H, PhH), 7.37 (dd, J = 8.7, 1.9 Hz, 1H), 7.18 (d, J = 2.3 Hz, 1H, furan-H). ^{13}C NMR (101 MHz, DMSO-d_6) δ 163.63 (d, J_{C-F} = 251.2 Hz), 157.42, 155.59 (dd, J_{C-F} = 248.6, 4.7 Hz), 155.03, 154.93, 151.63, 147.49 (d, J_{C-F} = 12.1 Hz), 141.85 (t, J_{C-F} = 2.3 Hz), 138.60 (t, J_{C-F} = 9.0 Hz), 133.93, 133.46, 128.81, 128.32, 127.97 (t, J_{C-F} = 16.2 Hz), 119.07, 115.22, 114.92 (d, J_{C-F} = 2.2 Hz), 112.20 (dd, J_{C-F} = 22.4, 5.0 Hz), 111.87, 107.85, 104.23 (d, J_{C-F} = 25.7 Hz), 90.91 (d, J_{C-F} = 15.5 Hz). HRMS Calcd. $C_{26}H_{13}F_3N_5O_2$ for $[M + H]^+$: 484.1016, found 484.1026.

*4′-((2-((4-Cyano-3-fluorophenyl)amino)furo[3,2-d]pyrimidin-4-yl)oxy)-3′,5′-dimethyl-[1,1′-biphenyl]-4-carbonitrile (**9**).* Off-white solid, yield: 89%, mp: 272.6−274.4 °C. ^{19}F NMR (376 MHz, DMSO-d_6) δ −106.86. ^{1}H NMR (400 MHz, DMSO-d_6) δ 10.27 (s, 1H, NH), 8.45 (d, J = 2.2 Hz, 1H, furan-H), 7.96−7.87 (m, 4H, PhH), 7.67 (s, 1H, PhH), 7.63 (s, 2H, PhH), 7.51 (t, J = 8.3 Hz, 1H, PhH), 7.31 (dd, J = 8.8, 2.0 Hz, 1H, PhH), 7.12 (d, J = 2.2 Hz, 1H, furan-H), 2.18 (s, 6H, diMe). ^{13}C NMR (101 MHz, DMSO-d_6) δ 163.6 (d, J_{C-F} = 251.1 Hz), 156.4, 155.2, 154.0, 152.6, 150.0, 147.8 (d, J_{C-F} = 12.3 Hz), 144.4, 136.6, 133.6, 133.2, 131.6, 129.4, 128.1, 127.9, 119.3, 115.3, 114.7 (d, J_{C-F} = 2.2 Hz), 110.4, 107.7, 104.0 (d, J_{C-F} = 25.8 Hz), 90.4 (d, J_{C-F} = 15.6 Hz), 16.7. HRMS Calcd. $C_{28}H_{19}FN_5O_2$ for $[M + H]^+$: 476.1517, found 476.1515.

*5-((4-((4′-Cyano-3,5-dimethyl-[1,1′-biphenyl]-4-yl)oxy)furo[3,2-d]pyrimidin-2-yl)amino)picolinonitrile (**10**).* Off-white solid, yield: 87% (purity: 97%), mp: 264.1−265.9 °C. ^{1}H NMR (400 MHz, DMSO-d_6) δ 10.18 (s, 1H, NH), 8.79 (d, J = 2.3 Hz, 1H, PhH), 8.46 (d, J = 2.2 Hz, 1H, furan-H), 8.14 (dd, J = 8.8, 2.3 Hz, 1H, PhH), 7.94 (s, 4H, PhH), 7.64 (s, 2H, PhH), 7.59 (d, J = 8.8 Hz, 1H, PhH), 7.13 (d, J = 2.2 Hz, 1H, furan-H), 2.19 (s, 6H, diMe). ^{13}C NMR (101 MHz, DMSO-d_6) δ 156.3, 155.3, 153.9, 152.7, 150.0, 144.5, 141.7, 141.2, 136.6, 133.3, 131.8, 129.5, 129.4, 128.1, 128.0, 123.6, 123.3, 119.3, 118.6, 110.5, 107.8, 16.7. HRMS Calcd. $C_{27}H_{19}N_6O_2$ for $[M + H]^+$: 459.1564, found 459.1567.

4.2. *In vitro anti-HIV-1 assay*

All the biological data were conducted at the Rega Institute for Medical Research, KU Leuven, Belgium, supervised by Prof. Erik De Clercq. All the compounds were evaluated to exhibit antiviral activity and cytotoxicity against WT HIV-1 (IIIB) and mutant strains, including L100I, K103N, Y181C, Y188L, E138K, F227L + V106A and RES056 in MT-4 cell cultures using MTT method. Exponentially growing MT-4 cells were dispensed into 96-well microtiter tray wells, followed by adding the serial diluted virus stocks using a Biomek 3000 robot (Beckman Instruments, Fullerton, CA) to identify 100−300 $CCID_{50}$ (50% cell culture infective dose). Compounds were dissolved in the DMSO stock (10 × final concentration) and then serially diluted to the standard concentrations ranging from 125, 25, 5, 1, 0.2, 0.04, 0.008 to 0.0016 μg/mL. Control groups included untreated HIV-infected and mock-infected cells. Mock-infected cells were used to assess the cytotoxicity of the tested compounds on uninfected cells. After different viral stocks (100−300 $CCID_{50}$, 50 μL) of wild-type and mutant strains or culture medium being added to the corresponding infected or mock-infected 96-wells, respectively, followed by diverse compound's concentrations. Then the exponentially growing MT-4 cells went through centrifugation and resuspension at a concentration of 6×10^5 cells/mL, subsequently the suspension (50 μL) was diverted into each microtiter well above. The system was incubated in an ambient environment of 5% CO_2, ≥95% relative humidity at 37 °C for 5 days. The cell viability was measured by the MTT assay. EC_{50} (50% effective concentration) was defined as a concentration that achieved 50% protection from the viral cytopathic effect in infected cells. CC_{50} (50% cytotoxic concentration) was referred to a concentration that led to 50% reduction of the viability of mock-infected MT-4 cells.

4.3. *HIV-1 RT inhibition assay*

Recombinant WT p66/p51 HIV-1 RT was expressed and purified in-house as previously described[30]. The ability of all compounds to inhibit HIV-1 RT was evaluated according to the procedure of the EnzCheck Reverse Transcriptase Assay kit (Molecular Probes, Invitrogen). The assay was based on the PicoGreen dsDNA quantitation reagent, which presented a significant increase in fluorescence signal once binding to dsDNA or RNA-DNA heteroduplexes while binding to single-stranded nucleic acids only evoked minimal fluorescence signal increase. This condition was met in the assay. A poly(A) template of approximately 350 bases long was annealed with an oligo(dT)16 primer at a molar ratio of 1:1.2 (room temperature for 60 min). 52 ng of RNA/DNA hybrid was added to each well of a 96-well plate, with a total volume of 20 μL polymerization buffer (containing 60 mmol/L Tris-HCl, 60 mmol/L KCl, 8 mmol/L $MgCl_2$, 13 mmol/L DTT, 100 μmol/L dTTP, pH 8.1). Prior to adding RT enzyme solution (25 nmol/L), 1.0 μL of tested compounds in DMSO at concentrations ranging from 0.0015 to 120 μg/mL were added to the above wells, control wells with equivalent volume of DMSO were also included. Subsequently, 5 μL of RT solution, diluted to an appropriate concentration in enzyme dilution buffer (containing 50 mmol/L Tris-HCl, 20% glycerol, 2 mmol/L DTT, pH 7.6) was added. After incubation at 25 °C for 40 min, the reaction mixture was quenched by adding EDTA (15 mmol/L) and subsequently detected using PicoGreen. A spectrofluorometer (Safire 2, Tecan) was applied to measure the fluorescence signal using 490 nm as an excitation wavelength and meanwhile 523 nm as an emission wavelength. Consequently, the biological results were expressed as the relative fluorescence that the fluorescence signal of the compound was divided by the signal of the control group.

4.4. *Molecular docking*

Molecular docking was performed on the Schrödinger Maestro 11.4, including the process of protein preparation (Protein Preparation Wizard), ligand preparation (LigPrep), receptor grid generation, and docking. The protein structures were retrieved from the Protein Data Bank, including WT HIV-1 RT (PDB ID: 6C0N or 2ZD1), F227L + V106A RT (PDB ID: 6DUF or 2ZD1),

RES056 RT (PDB ID: 6C0R or 2ZD1), meanwhile L100I, Y181C and Y188L RT mutants were generated from site-directional mutagenesis of WT HIV-1 RT (PDB ID: 6C0N) and subsequently went through regular processes above. Specifically, a standard protocol as follows: (1) assign bond orders, add hydrogen atoms, create zero-order bonds to metals; (2) exclude most of crystallographic waters and maintain a few potential waters; (3) H-bond assignment, sample water orientations and use PROPKA; (4) perform restrained minimization using OPLs_2005 force field; (5) use glide generation module to obtain Glide; (6) the docking module employ standard precision (SP) setting to make small molecule flexibly dock into its protein without constraints. Molecular docking results were visualized using PyMol (http://pymol.sourceforge.net/).

4.5. MD dynamic simulations

The binding stability of protein-ligand complexes between **7w** and WT HIV-1 RT (PDB ID: 6C0N), between **10** and WT HIV-1 RT (PDB ID: 2ZD1) were evaluated using molecular dynamics (MD) simulations employing the OPLS4 force field with the Desmond package (Schrödinger 11.4). The complex was filled in a water orthorhombic periodic box with a minimum distance of 10 Å between the protein and the box boundaries. The system was neutralized by adding extra Na^+ ion and Cl^- counterions (about a 0.15 mol/L NaCl concentration) to simulate physiological conditions *via* the Desmond System Builder setting. Next the solvated system was minimized and equilibrated through OPLS4 force field parameters on the Desmond default protocols. Subsequently, the NPT ensemble was set at isothermal isobaric conditions with 300K temperature and 1.0325 bar pressure. The simulation ran for 100 ns with trajectory frames captured for every 50 ps. The MD trajectories were analyzed by the Desmond Simulation Interaction Diagram (SID) to deduce the ligand's binding orientation.

4.6. hERG channel qpatch assay

Compound **10**, dissolved firstly in DMSO, was prepared in 20 mmol/L of stock solution and preserved in freezing condition. The stock solution was able to thaw at the beginning of the assay, and then was serially diluted by 3 times in DMSO to obtain a working solution. The working solution was further diluted by 500 times to get a desired final concentration in external culture medium. It should be noted that the final concentration of DMSO is kept at 0.2% so that it would not affect the human ether-ago-go-related gene (hERG) potassium channel. The hERG-CHO cell line, developed in house, was incubated in T75 culture flasks at 37 °C under the condition of 5% CO_2. The growth medium consisted of F-12 medium (Invitrogen 11765062, ThermoFisher, USA) filled with 10% fetal bovine serum (Invitrogen 10099141, ThermoFisher, USA), 100 μg/mL G418 (Invitrogen 11811023, ThermoFisher, USA), and 100 μg/mL Hygromycin B (Invitrogen 10687010, ThermoFisher, USA) and this kind of growth medium was added to the cells, followed by addition of 7 mL PBS. The cells were treated with 3 mL of Detachin reagent at 37 °C for 3 min in order to remove them from the culture bottle. About 7 mL of culture medium was added to the bottle to resuspend the cells, the resulting suspension was further centrifuged at a speed of 800 rpm for several minutes and were collected. The cell density for automatic Qpatch 16x experiments was adjusted to 2−5 million cells/mL using Sophion's QPatch 16x system from Denmark. The hERG channel current was measured on automatic QPatch 16x equipped with a single-hole QPlate using the whole-cell patch clamp technique. The cell's holding potential was maintained at −80 mV, once activating, it was depolarized to +20 mV for 5 s, then repolarized to −50 mV for 5 s to eliminate inactivation and observe the deactivated tail current. The hERG current was measured by calculating the amplitude of the peak tail current (QT interval). Each concentration of **10** was tested on three groups of cells and the raw data were filtered to screen just records that membrane resistance (Rm) was greater than 100 MΩ and tail current amplitude was more than 300 pA, compared with control conditions.

4.7. Cytochrome P450 inhibition assay

The assay was conducted in a 96-well plate, with a final incubation volume of 100 μL each well. Each well contained 20 μL of human liver microsomes (HLM, with a final concentration of 0.3 mg/mL), 50 μL of the test compound **10** or positive control inhibitor and 20 μL of probe substrate dissolved in 0.1 mol/L Tris (pH 7.4). After preincubation at 37 °C for 10 min, added 10 μL of NADPH (co-enzyme II) to the reaction mixture being a final concentration of 1 mmol/L to initiate the reaction. After incubation at 37 °C for 15 min, the reaction was quenched by adding 100 μL of acetonitrile containing 50 nmol/L of internal standards (propranolol, nadolol). Then the reaction plate was centrifuged and the supernatant was analyzed by LC/MS/MS. The positive control inhibitors included nifedipine, quinidine and ketoconazole, respectively. In addition, phenacetin, tolbutamide, *s*-mephenytoin, dextromethorphan, testosterone and midazolam were used as probe substrates, because they were able to selectively inhibit CYP1A2, CYP2C9, CYP2C19, CYP2D6, and CYP3A4 enzymes respectively.

4.8. PK study

All protocols involving animal experimental subjects strictly followed the guidelines outlined in the National Institutes of Health's "Guidelines for the Care and Use of Laboratory Animals". In addition, this study strictly followed an authorized animal experimental protocol (2020CHEM-JS-005) approved by the Animal Care Committee of Fudan University at all stages. Six male Sprague−Dawley rats (SPF grade) were transferred from the institutional animal repository (No. 999M-017), Beijing Vital River Laboratory Animal Technology Co., Ltd. located in Beijing, China. The experimental animals had free access to food and water under a 12-h light/dark cycle, followed by a 10-h fasting period prior to dosing and feeding 4 h after administration. Rats were divided into two groups ($n = 3$) to receive either intravenous injection at a dose of 1 mg/kg or oral administration at a dose of 10 mg/kg. The sample **10** was solved in a colorless, clear solution or homogeneous suspension, respectively, in solution (5% DMSO+10% solutol+85% saline) before the experiment. For intravenous group, blood samples (200 μL/per) were collected at specifical time intervals (0.083, 0.25, 0.5, 1, 2, 4, 8 and 24 h) from the sinus jugular or other suitable method into centrifuge tubes pretreated with K_2-EDTA, while blood samples were collected at time intervals (0.25, 0.5, 1, 2, 4, 8 and 24 h) for oral administration group. Simultaneously, blood collection requirements and handling as followed: utilizing anticoagulant K_2-EDTA tubes and standing in a wet ice environment for more than 15 min. Then the mixture was centrifuged for 6 min at 6800×*g* at 2−8 °C to separate plasma, which was stored in the refrigerator (−80 °C) for testing. Then sample preparation as followed: an aliquot of 40 μL plasma sample was protein precipitated with 400 μL MeOH in

which contains 100 ng/mL Warfarin (IS). The mixture was vortexed for 1 min. Then for samples treated with tube were centrifuged at 14,000 rpm for 7 min, but for samples treated with 96 well plates were centrifuged at 4000 rpm for 10 min. Transfer 380 μL supernatant to 96 well plates. An aliquot of 10 μL supernatant was injected for LC−MS/MS analysis. The bioanalytical method and the analysis of all samples were completed by the DMPK Bioanalytical Laboratory at Medicilon (Shanghai) MedPearl Technology Co., Ltd. During sample analysis, the within-run accuracy of quality control (QC) samples was evaluated, with the requirement that more than 66.7% of all QC samples and at least 50% of the QC samples at each concentration level must have an accuracy within the range of 80% to 120%. The standard curve of **10** was plotted by mixing its different concentrations with a blank plasma and adding Warfarin (IS) as an internal standard. All blood samples were quantitative analyzed using LC−MS/MS-23 (TQ6500+) equipped with multiple reaction monitoring (MRM) technique. Then acetonitrile (+0.1% formic acid)/water (+0.1% formic acid) gradient solution was used as the mobile phase at a flow rate of 0.6 mL/min using chromatography column (Acquity UPLC CSH C18 1.7 μm 2.1 mm × 50 mm). The pharmacokinetic parameters, including AUC_{0-t}, $AUC_{0-\infty}$, $MRT_{0-\infty}$, C_{max}, T_{max}, and $t_{1/2}$, were calculated based on blood concentration data at different time points using Phoenix WinNonlin® version 7.0 or higher. Mean values and standard deviations are provided for each parameter.

Acknowledgments

This work was financially supported by the National Natural Science Foundation of China (Nos. 82574236 and 82304297), Shanghai Pujiang Programme (No. 23PJD005) and the State Key Laboratory of Natural and Biomimetic Drugs (No. K202408, China).

Author contributions

Yin-Xiang Zhang, Xu-Dong Li, Phuong-Thao Tran, and Shuai Wang conducted the design and synthesis of compounds. Yin-Xiang Zhang and Shuai Wang supervised the druglikeness evaluation experiment and were responsible for writing. Shuo Su, Erik De Clercq, Christophe Pannecouque, Laura Dettori, Angela Corona, and Enzo Tramontano completed the biological evaluation assays. Shuai Wang and Fen-Er Chen conceived the project and provided resources, supervision, and financial support. All authors critically evaluated the manuscript prior to submission.

Conflicts of interest

The authors declared no conflicts of interest.

Appendix A. Supporting information

Supporting information to this article can be found online at https://doi.org/10.1016/j.apsb.2026.01.010.

References

1. Cilento ME, Kirby KA, Sarafianos SG. Avoiding drug resistance in HIV reverse transcriptase. *Chem Rev* 2021;**121**:3271−96.
2. Zhang K, Zhao L, Xing T, Bu Y, Wang Q, Pannecouque C, et al. Rational structure-based design and optimization of next-generation biphenyl-piperidine-triazine derivatives as potent non-nucleoside reverse transcriptase inhibitors. *Chin Chem Lett* 2025:111283.
3. Zhuang C, Pannecouque C, De Clercq E, Chen F. Development of non-nucleoside reverse transcriptase inhibitors (NNRTIs): our past twenty years. *Acta Pharm Sin B* 2020;**10**:961−78.
4. Hu WS, Hughes SH. HIV-1 reverse transcription. *Cold Spring Harb Perspect Med* 2012;**2**:a006882.
5. Wang Z, Cherukupalli S, Xie M, Wang W, Jiang X, Jia R, et al. Contemporary medicinal chemistry strategies for the discovery and development of novel HIV-1 non-nucleoside reverse transcriptase inhibitors. *J Med Chem* 2022;**65**:3729−57.
6. Poongavanam V, Namasivayam V, Vanangamudi M, Al Shamaileh H, Veedu RN, Kihlberg J, et al. Integrative approaches in HIV-1 non-nucleoside reverse transcriptase inhibitor design. *WIREs Comput Mol Sci* 2017;**8**:e1328.
7. Namasivayam V, Vanangamudi M, Kramer VG, Kurup S, Zhan P, Liu X, et al. The journey of HIV-1 non-nucleoside reverse transcriptase inhibitors (NNRTIs) from lab to clinic. *J Med Chem* 2018;**62**:4851−83.
8. Lansdon EB, Brendza KM, Hung M, Wang R, Mukund S, Jin D, et al. Crystal structures of HIV-1 reverse transcriptase with etravirine (TMC125) and rilpivirine (TMC278): implications for drug design. *J Med Chem* 2010;**53**:4295−9.
9. Huang WJ, Pannecouque C, De Clercq E, Corona A, Maloccu S, Tramontano E, et al. Expanding the solvent/protein region occupation of the non-nucleoside reverse transcriptase inhibitor binding pocket for improved broad-spectrum anti-HIV-1 efficacy: from rigid phenyl-diarylpyrimidines to flexible hydrophilic piperidine-diarylpyrimidines. *J Med Chem* 2024;**67**:19889−904.
10. Haubrich R, Gubernick S, Yasothan U, Kirkpatrick P. Etravirine. *Nat Rev Drug Discov* 2008;**7**:287−8.
11. Sanford M. Rilpivirine. *Drugs* 2012;**72**:525−41.
12. Chen XM, Hao QQ, Pannecouque C, De Clercq E, Wang S, Chen FE. Bioisosterism-driven design of orally active, safe, and broad-spectrum biphenyl-DAPY derivatives as highly potent HIV-1 non-nucleoside reverse transcriptase inhibitors. *Acta Pharm Sin B* 2025;**15**:4115−36.
13. Ripamonti D, Bombana E, Rizzi M. Rilpivirine: drug profile of a second-generation non-nucleoside reverse transcriptase HIV-inhibitor. *Expert Rev Anti Infect Ther* 2013;**12**:13−29.
14. Johnson BC, Pauly GT, Rai G, Patel D, Bauman JD, Baker HL, et al. A comparison of the ability of rilpivirine (TMC278) and selected analogues to inhibit clinically relevant HIV-1 reverse transcriptase mutants. *Retrovirology* 2012;**9**:99.
15. Lambert-Niclot S, Charpentier C, Storto A, Fofana D, Soulie C, Fourati S, et al. Rilpivirine, emtricitabine and tenofovir resistance in HIV-1-infected rilpivirine-naive patients failing antiretroviral therapy. *J Antimicrob Chemother* 2014;**69**:1086−9.
16. Huang J, Pannecouque C, De Clercq E, Wang S, Chen FE. Structure-based discovery of novel piperidine-biphenyl-DAPY derivatives as non-nucleoside reverse transcriptase inhibitors featuring improved potency, safety, and selectivity: from piperazine-biphenyl-DAPYs to piperidine-biphenyl-DAPYs. *Eur J Med Chem* 2024;**276**:116668.
17. Zhang T, Yang Y, Li X, Zhao F, Zhuo Z, Wang L, et al. Probing the dominant motifs within the hydrophobic channel yields oxadiazole-containing diarylpyrimidine derivatives as potent HIV-1 non-nucleoside reverse transcriptase inhibitors. *J Med Chem* 2025;**68**:16197−211.
18. Zhang K, Xing T, Ding L, Pannecouque C, De Clercq E, Corona A, et al. Deuteration strategy-inspired design of novel diarylpyrimidine derivatives as potent non-nucleoside reverse transcriptase inhibitors featuring improved efficacy, selectivity, and druggability. *J Med Chem* 2025;**68**:8564−77.
19. Ji X, Jiang X, Gao Z, Gao H, Huang X, Zhao F, et al. Exploring the HIV-1 reverse transcriptase p51/p66 interface: structure-based design and optimization of novel 2,4,6-trisubstituted pyrimidines as potent NNRTIs with improved resistance profiles. *J Med Chem* 2025;**68**:20519−35.
20. Garrido A, Lepailleur A, Mignani SM, Dallemagne P, Rochais C. hERG toxicity assessment: useful guidelines for drug design. *Eur J Med Chem* 2020;**195**:112290.

21. Chen XM, Xu Q, Pannecouque C, De Clercq E, Tramontano E, Tran PT, et al. Halogenation-driven discovery of halomethylene-biphenyl-diarylpyrimidines as potent HIV-1 non-nucleoside reverse transcriptase inhibitors with improved safety and PK profiles. *J Med Chem* 2025;**68**: 15358−71.
22. Kang D, Ruiz FX, Feng D, Pilch A, Zhao T, Wei F, et al. Discovery and characterization of fluorine-substituted diarylpyrimidine derivatives as novel HIV-1 NNRTIs with highly improved resistance profiles and low activity for the hERG ion channel. *J Med Chem* 2020;**63**:1298−312.
23. Kang D, Sun Y, Murugan NA, Feng D, Wei F, Li J, et al. Structur-e−activity relationship exploration of NNIBP tolerant region I leads to potent HIV-1 NNRTIs. *ACS Infect Dis* 2020;**6**:2225−34.
24. Heffron TP, Wei B, Olivero A, Staben ST, Tsui V, Do S, et al. Rational design of phosphoinositide 3-kinase α inhibitors that exhibit selectivity over the phosphoinositide 3-kinase β isoform. *J Med Chem* 2011;**54**:7815−33.
25. Srimongkolpithak N, Sundriyal S, Li F, Vedadi M, Fuchter MJ. Identification of 2,4-diamino-6,7-dimethoxyquinoline derivatives as G9a inhibitors. *MedChemComm* 2014;**5**:1821−8.
26. Wu Z, Bai Y, Jin J, Jiang T, Shen H, Ju Q, et al. Discovery of novel and potent PARP/PI3K dual inhibitors for the treatment of cancer. *Eur J Med Chem* 2021;**217**:113357.
27. Yang M, Liu Y, Qi X, Zhao Y, Wu XF. Carbonylative transformation of aryl halides and strong bonds *via* cheap metal catalysts and sustainable technologies. *Green Synth Catal* 2024;**5**:211−69.
28. Qiu B, Shi YF, An XD, Guo SK, Shen YB, Xiao J. Divergent synthesis of new naphtho-fused 2-aminoindolines and naphthoxindoles based on straightforward construction of phenanthrene. *Green Synth Catal* 2025;**6**: 110−3.
29. Pannecouque C, Daelemans D, De Clercq E. Tetrazolium-based colorimetric assay for the detection of HIV replication inhibitors: revisited 20 years later. *Nat Protoc* 2008;**3**:427−34.
30. Auwerx J, North TW, Preston BD, Klarmann GJ, De Clercq E, Balzarini J. Chimeric human immunodeficiency virus type 1 and feline immunodeficiency virus reverse transcriptases: role of the subunits in resistance/sensitivity to non-nucleoside reverse transcriptase in-hibitors. *Mol Pharmacol* 2002;**61**:400−6.